NASA Technical Memorandum 107028

Turbulent Fluid Motion VI—
Turbulence, Nonlinear Dynamics, and Deterministic Chaos

Robert G. Deissler
Lewis Research Center
Cleveland, Ohio

September 1996

National Aeronautics and
Space Administration

PREFACE

Researchers have been active in serious studies of turbulence for more than a century. Today, as it was a century ago, turbulence is ubiquitous. But although it is still an active field of research, there is no general deductive theory of strong turbulence.

The literature on turbulence is now far too voluminous for anything like a full presentation to be given in a moderately-sized volume. Rather it will be attempted here to give a coherent account of one line of development. Part of this has been given in abbreviated form in Chapter 7 of Handbook of Turbulence, Volume 1 (Plenum, 1977). In particular, the scope of the work, which was somewhat limited by our inability to solve the fundamental nonlinear equations, has been considerably increased by numerical solutions. Moreover, applications of dynamical systems theory in conjunction with numerical solutions have resulted in, among other things, a sharper characterization of turbulence and a deliniation of routes to turbulence.

Throughout the book the emphasis will be on understanding the physical processes in turbulent flow. This will be done to a large extent by obtaining and interpreting analytical or numerical solutions of the equations of fluid motion. No attempt will be made to either emphasize or avoid the use of mathematical analysis. Since most of the material is given in some detail, the student or research worker with a modest knowledge of fluid mechanics should not find the text particularly hard to follow. Some familiarity with Cartesian-tensor notation and Fourier analysis may be helpful, although background material in those subjects will be given.

Although turbulence, as it occurs, is more often strong than weak, it appears that much can be learned about its nature by considering weak or moderately weak turbulence, as is often done here. In general, the same processes occur in moderately weak turbulence as occur at much higher Reynolds numbers; the differences are quantitative rather than qualitative. The crux of the matter might therefore be accessible through low and moderate Reynolds-number studies.

The basis of the present account of turbulence is the Navier-Stokes and other continuum equations for fluids. It is hoped that the book will show how those equations can act as a unifying thread for such an account.

Some introductory material on fluid turbulence is presented in chapter I. This includes discussions and illustrations of what turbulence is, and how, why, and where turbulence occurs. Then, in chapter II, some of the mathematical apparatus used for the representation and study of turbulence is developed.

A derivation of the continuum equations used for the analysis of turbulence is given in chapter III. These equations include the continuity equation, the Navier-Stokes equations, and the heat-transfer or energy equation. An experimental justification for using a continuum approach for the study of turbulence is also given.

Ensemble, time, and space averages as applied to turbulent quantities are discussed in chapter IV, and pertinent properties of the averages are obtained. Those properties, together with Reynolds decomposition, are used to derive the averaged equations of motion and the one- and two-point moment or correlation equations. The terms in the various equations are interpreted. The closure problem of the averaged equations is discussed, and possible closure schemes are considered. Those schemes usually require an input of supplemental information, unless the averaged equations are closed by calculating their terms by a numerical solution of the original unaveraged equations. The law of the wall for velocities and for temperatures, the velocity- and temperature-defect laws, and the logarithmic laws for velocities and for temperatures are derived. Various notions of randomness and their relation to turbulence are considered in the light of modern ergodic theory.

Background material on Fourier analysis and on the spectral form of the continuum equations, both averaged and unaveraged, are given in chapter V. The equations are applied to a number of cases of homogeneous turbulence with and without mean gradients. Some turbulent solutions of the full unaveraged continuum equations are obtained numerically. Closure of the averaged equations by specification of sufficient random initial conditions is considered. The gap problem (the problem of bridging the gap between the infinite amount of data required to specify an initial turbulence and the finite amount generally available) is discussed. Then a solution for the evolution of all of the quantities used to specify the initial turbulence is obtained. Spectral transfer of turbulent activity between scales of motion is studied in some detail. The effects of mean shear, heat transfer, normal strain, and buoyancy are included in the analyses.

Finally, in chapter VI the unaveraged Navier-Stokes equations are used numerically in conjuction with tools and concepts from nonlinear dynamics, including time series, phase portraits, Poincaré sections, Liapunov exponents, power spectra, and strange attractors. Initially neighboring solutions for a low Reynolds-number fully developed turbulence are compared, where the turbulence is sustained by a nonrandom time-independent external force. By reducing the Reynolds number (forcing), several nonturbulent solutions are also obtained and contrasted with the turbulent ones.

I should like to thank F.B. Molls for his work on the calculations, and R.J. Deissler, E. Reshotko, I. Greber, Y. Kamotani, N. Mhuiris, and F. McCaughan for helpful discussions in connection with the studies in chapter VI.

TURBULENT FLUID MOTION VI—

Turbulence, Nonlinear Dynamics, and Deterministic Chaos

Robert G. Deissler
National Aeronautics and Space Administration
Lewis Research Center
Cleveland, Ohio 44135

SUMMARY

Several turbulent and nonturbulent solutions of the Navier-Stokes equations are obtained. The unaveraged equations are used numerically in conjunction with tools and concepts from nonlinear dynamics, including time series, phase portraits, Poincaré sections. Liapunov exponents, power spectra, and strange attractors.

Initially neighboring solutions for a low Reynolds-number fully developed turbulence are compared. The turbulence is sustained by a nonrandom time-independent external force. The solutions, on the average, separate exponentially with time, having a positive Liapunov exponent. Thus, the turbulence is characterized as chaotic.

In a search for solutions which contrast with the turbulent ones, the Reynolds number (or strength of the forcing) is reduced. Several qualitatively different flows are noted. These are, respectively, fully chaotic, complex periodic, weakly chaotic, simple periodic, and fixed-point. Of these, we classify only the fully chaotic flows as turbulent. Those flows have both a positive Liapunov exponent and Poincaré sections without pattern. By contrast, the weakly chaotic flows, although having positive Liapunov exponents, have some pattern in their Poincaré sections. The fixed-point and periodic flows are nonturbulent, since turbulence, as generally understood, is both time-dependent and aperiodic.

INTRODUCTION

As is apparent from the preceding chapters, fluid turbulence is a many-faceted phenomenon. It has been characterized as random, nonlinear, multiscaled, dissipative, as having a negative velocity-derivative skewness factor, as transferring energy (mainly) to small-scale motions, as being dissipated by small-scale motions, as tending toward isotropy, and as having an infinite number of components or degrees of freedom. Those descriptions appear in what might now be called the classical or statistical theory of turbulence (refs. 1 to 5). That theory is based mainly on averaged or moment equations obtained from the Navier-Stokes equations.

It was mentioned in the introductory remarks of chapter IV that the idea of using averaged equations, rather than the unaveraged Navier-Stokes equations directly in an analysis, has been adopted in the past mainly because it was thought that averaged, smoothly varying quantities should be easier to deal with than the haphazard motions occurring in the unaveraged equations. However because of the nonlinearity of the Navier-Stokes equations, the averaging process introduces the closure problem (more unknowns than equations (chapter IV), so that it is not clear that averaging is advantageous as far as getting solutions is concerned.[1] The averaged or moment equations are, however, useful (if not necessary) for discussing the physical processes occurring in turbulence (see chapters IV and V).

In recent years there have been attempts to utilize concepts from the theory of nonlinear dynamical systems in the analysis of turbulence (refs. 6 to 12). There, in contrast to the statistical theory, the emphasis is on unaveraged, rather than on averaged equations. The use of unaveraged equations in which the velocities vary in a complicated way is made feasible by the advent of high speed computers. By using ideas from nonlinear dynamics one might (as further evidence that turbulence is a many-faceted phenomenon) characterize turbulence as chaotic although deterministic, as aperiodic, as having sensitive dependence on initial conditions, as having time series without pattern, as having a positive Liapunov exponent, as having a phase portrait without pattern, as having Poincaré sections without pattern, as lying on a strange or chaotic attractor, and as having continuous time and spatial spectra.

[1]Recall that parts of chapters IV and V were devoted to numerical solutions of the *unaveraged* equations.

Both the statistical (classical) theory and the newer nonlinear dynamics theory provide valid ways of looking at turbulence. The latter furnishes a number of new tools for probing the nature of turbulence (e.g., Liapunov exponents, Poincaré sections, etc.). But as yet it does not seem to provide a means of discussing such well-known aspects of turbulence as spectral and directional transfer of energy. Those aspects can, however, be considered within the framework of conventional turbulence theory (see chapter V).

Here we study the nature of Navier-Stokes turbulence (the turbulence obtained from solutions of the Navier-Stokes equations) by using concepts from nonlinear dynamics. Sensitive dependence on initial conditions and strange (chaotic) attractors are included. These are shown to occur in turbulence by obtaining and interpreting (mainly numerical) solutions of the Navier-Stokes equations.

In order to give a sharper characterization of turbulence, turbulent solutions are contrasted with periodic, quasiperiodic, and fixed-point solutions. Turbulent systems are also compared with those considered in the kinetic theory of gases. There is a certain suddenness inherent in turbulent mixing (section 4.3.2.3), as there is in molecular mixing by collision of gas particles.

Before investigating turbulence, we will consider a low-order system. We will see that solutions of that system have similarities to high (infinite)-order turbulence.

6.1 A LOW-ORDER NONLINEAR SYSTEM

An important (and surprising) result from nonlinear dynamics studies is that highly complex or chaotic motion can be obtained in systems with only a few (but not less than three) modes or degrees of freedom.[2] The best known low-order example is the Lorenz system (ref. 12):

$$\frac{d}{dt}\begin{bmatrix} x \\ y \\ z \end{bmatrix} = \begin{bmatrix} s(y-x) \\ rx - xz - y \\ xy - bz \end{bmatrix}, \qquad (6-1)$$

where t is the time and x, y, z are the three degrees of freedom of the system.

The variable (mode) y in equation (6-1) is plotted against time t in figure 6-1, where b = 1, r = 26, and s = 3. The initial conditions are given by x = 0, y = 1, and z = 0 at t = 0. The quantity plotted in figure 6-1 has a random appearance, in spite of the fact that the system has only three degrees of freedom. In fact, the flow in figure 6-1 is somewhat like that in figure 1-3, where a component of *turbulence* for a particular experimental flow is plotted against time; both flows have a random appearance. This is perhaps unexpected, since turbulence is described by partial differential equations (the Navier-Stokes equations) and thus has (theoretically) an *infinite* number of degrees of freedom. The random appearance of turbulence has been ascribed to the infinite number of degrees of freedom (refs. 13 to 15), but it now appears that as few as three are sufficient.

Comparison of figures 6-1(a) and (b) shows the effect of a small change in initial condition. A change in initial y of 0.1 percent produces a very large change in y at times beyond the indicated time of breakaway from the unperturbed flow, although there is no perceptible change at earlier times. The flow thus appears to be sensitively dependent on initial conditions—a necessary (although not sufficient) condition for a flow to be turbulent. This is another indication of the similarity of the low-order flow in figure 6-1 to a turbulent flow.

Finally, by comparing figures 6-1(b) and (c) we investigate the effect of time increment Δt in the numerical solution of the Lorenz system on the evolution of y. An improved Euler method (ref. 16) was used in the numerical solution. Increasing Δt from 0.002 in figures 6-1(b) to 0.01 in figure 6-1(c) (with everything else held constant) has no perceptible effect on the evolution of y for times smaller than the breakaway time indicated in figure 6-1(c). Thus, the numerical calculations in the two graphs (figs. 6-1(b) and (c)) are accurate in the usual sense. But for times

[2]It turns out that at least three modes are necessary if a chaotic solution is to be unique (ref. 7). If say only two modes (or dimensions in phase or state space) were present, a chaotic solution in phase space would intersect itself and thus not be unique.

greater than the breakaway time the evolutions are completely different, apparently because of the inherent instability or chaoticity of the system for the parameters shown. Thus, the effect of increasing Δt is qualitatively similar to that of giving a small perturbation to the initial condition.

Following this brief study of a low-order chaotic system we go now to the Navier-Stokes system (ref. 17). As in the preceding chapters the Navier-Stokes equations are used to describe turbulence in fluids.

6.2 BASIC EQUATIONS AND A LONG-TERM TURBULENT SOLUTION WITH STEADY FORCING

The incompressible Navier-Stokes equations, on which the present study is based, are

$$\frac{\partial u_i}{\partial t} = -\frac{\partial (u_i u_k)}{\partial x_k} - \frac{1}{\rho}\frac{\partial \sigma}{\partial x_i} + \nu \frac{\partial^2 u_i}{\partial x_k \partial x_k} + F_i, \tag{6-2}$$

together with a Poisson equation for the pressure

$$\frac{1}{\rho}\frac{\partial^2 \sigma}{\partial x_\ell \partial x_\ell} = -\frac{\partial^2 (u_\ell u_k)}{\partial x_\ell \partial x_k} + \frac{\partial F_\ell}{\partial x_\ell}. \tag{6-3}$$

The subscripts can have the values 1, 2, or 3, and a repeated subscript in a term indicates a summation, with the subscript successively taking on the values 1, 2, and 3. The quantity u_i is an instantaneous velocity component, x_i is a space coordinate, t is the time, ρ is the density, ν is the kinematic viscosity, σ is the instantaneous (mechanical) pressure, and F_i is a time-independent forcing term, or external force, which is taken as some fraction χ of the negative of the initial viscous term at t = 0. That is,

$$F_i = -\chi \nu \left(\frac{\partial^2 u_i}{\partial x_k \partial x_k} \right)_{t=0}. \tag{6-4}$$

The fraction χ controls the value of the asymptotic Reynolds number of the flow. Equations (6-2) and (6-3) are respectively the same as equations (3-19) and (3-21) if the forcing term F_i is replaced by the body force g_i. The initial nonrandom u_i in equation (6-4) are given at t = 0 by

$$u_i = a_i \cos \mathbf{q}\cdot\mathbf{x} + b_i \cos \mathbf{r}\cdot\mathbf{x} + c_i \cos \mathbf{s}\cdot\mathbf{x}, \tag{6-5}$$

where

$$\begin{gathered} a_i = k(2,1,1), \quad b_i = k(1,2,1), \quad c_i = k(1,1,2), \\ q_i = (-1,1,1)/x_0, \quad r_i = (1,-1,1)/x_0, \quad s_i = (1,1,-1)/x_0, \end{gathered} \tag{6-6}$$

k is a quantity that fixes the initial Reynolds number at t = 0, and x_0 is one over the magnitude of an initial wavenumber component. Through equation (6-4), x_0 is also one over the magnitude of a wavenumber component of the forcing term F_i. Equations (6-5) and (6-6) satisfy continuity, and equations (6-2) to (6-4) insure that continuity is maintained. Moreover equations (6-4) to (6-6) give local values of F_i which are symmetric with respect to 90° rotations and translations of $2\pi x_0$. Then we find numerically that

$$\overline{u_1^2} \approx \overline{u_2^2} \approx \overline{u_3^2} \tag{6-7a}$$

at all times, where the overbars indicate values averaged over space. After the initial transients have died out, the averages may also be taken over time, and the inexact equalities in equation (6-7(a)) become equalities. Equation (6-7a) then becomes

$$\overline{\overline{u_1^2}} = \overline{\overline{u_2^2}} = \overline{\overline{u_3^2}}, \qquad (6-7b)$$

where the double bars indicate averages over space and time. The boundary conditions are periodic with a period of $2\pi x_0$. From equation (6-4) and continuity, the last term in equation (6-3) is zero for our system.

Equation (6-2) is a nonlinear dissipative equation for the evolution of the vector u_i. Although a Navier-Stokes fluid is linear (stress proportional to strain rate), a nonlinearity appears in equation (6-2) as an effect of inertia. The equation is autonomous, since time does not appear explicitly on the right side, and deterministic since there are no random coefficients. Note that the equation would not be autonomous if the forcing term F_i were time-dependent. Equation (6-2), although three-dimensional in physical space, is infinite-dimensional in phase (or state) space, since it is a partial differential equation. (The number of dimensions of the phase space of our system is the number of u_i's required to specify the velocity field at a particular time. The pressure is not specified; it is calculated from equation (6-3).) The equation can be converted to an infinite system of ordinary differential equations by, for instance, introducing finite-difference representations of spatial derivatives (and letting grid spacing approach 0), or by taking the spatial Fourier transform of the equation. Because it is dissipative, the infinite system can be represented by a finite system of equations (ref. 11). There should be a viscous cutoff, below which motion becomes unimportant as the scale of the motion decreases. Thus, a numerical solution should be possible, at least for low Reynolds numbers. Equation (6-2), together with equation (6-3) for the pressure, equations (6-4) to (6-6) for the forcing term, equations (6-5) and (6-6) for the initial conditions, and periodic boundary conditions, can be considered a nonlinear, deterministic, autonomous, dissipative, dynamical system. The system is deterministic, since there are no random elements in equations (6-2) to (6-6) or in the boundary conditions.

The numerical method used for the solution of equations (6-2) to (6-6) has been given in reference 18 and in section 5.3.2.6. A cubical computational grid (32^3 grid points), fourth-order spatial differencing, and third-order predictor-corrector time differencing are used. In order to obtain numerical stability for the highest asymptotic Reynolds number (13.3), it was necessary to use about 50 time steps in each small fluctuation of velocity, so that the fluctuations with respect to time are well resolved indeed. The spatial resolution is also good and will be discussed later, in connection with figure 6-6.

It follows from equations (6-4) to (6-6) that the nonrandom initial condition on u_i applied at $t = 0$ is proportional to the steady forcing term F_i. The quantity $(u_i)_{t=0}$, or F_i, on an $x_j - x_k$ plane through the numerical grid center is plotted in figure 6-2. Figure 6-3 shows the magnitude of the vector $(u_i)_{t=0}$ or F_i. A high degree of spatial symmetry of $(u_i)_{t=0}$ and of F_i is apparent from these plots. Note that as a result of the symmetry, the subscript i can designate any component of the vectors, and that the $x_j - x_k$ plane can be any plane through the numerical grid center parallel to the grid axes. That is, i,j, and k = 1,2, or 3; $j \neq k$. Moreover, the symmetry allows the development of symmetric turbulence in a box, where the box has periodic walls.

Results for the evolution of $\left(\overline{u_1^2}\right)^{1/2}$ for χ in equation (6-4) equal to 1 (asymptotic Reynolds number, 13.3) are given in figure 6-4 (see figure 6-4 for definition of the Reynolds number). The value of k in equation (6-6) is 20, giving an initial Reynolds number at $t = 0$ of 34.6. The velocities have been divided by $\left(\overline{u_0^2}\right)^{1/2}$, where the 0 again refers to $t = 0$. An asymptotic turbulent solution is obtained for $t^* > 5$. (The asterisk on t indicates that it has been nondimensionalized by x_0 and ν.)

A rather remarkable feature of turbulent flow is that a time-dependent haphazard flow can result when the applied exciting forces are steady (e.g., in a fully developed turbulent pipe flow with a steady applied pressure gradient). Figure 6-4 shows that the Navier-Stokes turbulence calculated here exhibits this feature, since a steady forcing term produces an apparently haphazard time-dependent motion. This is evidently the result of a kind of instability of the nonlinear Navier-Stokes equations except at very low Reynolds numbers, since initially neighboring solutions separate exponentially with time. That is, those solutions are chaotic (ref. 9). It will later be seen that our steady forcing term can also produce time-dependent *non*turbulent flow.

It should be mentioned that the symmetry present in the initial conditions (equations (6-5) and (6-6)) which, for instance, causes the three local velocity components to be equal for $x_1 = x_2 = x_3$ at $t = 0$, has been destroyed before $t^* = 5$, apparently by roundoff errors. This symmetry-breaking for local values must indeed occur in order for true turbulence to develop, and in fact the fluctuations eventually die out if the symmetry remains. Here the initial fluctuations were not strong enough to destroy the symmetry before the fluctuations become too small to be seen on the

u_1 curve. The symmetry-breaking apparently occurred on the flat portion of the curve by the accumulation of roundoff errors. For higher initial Reynolds numbers (not shown) the initial fluctuations were strong enough to break the local symmetry earlier, and the flat portion of the u_1 curve was absent.

The mean skewness factor S of the velocity derivative of our Navier-Stokes turbulence in figure 6-4 is calculated to be

$$S = \overline{\left(\frac{\partial u_1}{\partial x_1}\right)^3} \Bigg/ \left[\overline{\left(\frac{\partial u_1}{\partial x_1}\right)^2}\right]^{3/2} = -0.52, \qquad (6-8)$$

where the skewness factor is averaged over time after the powers of the velocity derivative have been averaged over space. This value is close to those obtained experimentally for a variety of simple turbulent flows (ref. 19), where the Reynolds numbers of the experiments were in the same range as that for the solution in figure 6-4.

Instantaneous (unaveraged) terms in the Navier-Stokes equation (equation (6-2)) for i = 1 at the numerical grid center are plotted in figure 6-5. These include the nonlinear convective term $-\partial(u_i u_k)/\partial x_k$, the steady forcing term F_i, the viscous term $\nu\partial^2 u_i/\partial x_k \partial x_k$, and the pressure term $-(1/\rho)\partial\sigma/\partial x_i$.

For the asymptotic or developed region (for $t^* > 5$) the viscous term is of the same order of magnitude as the steady forcing term. This is reasonable since the forcing term replenishes the energy lost by viscous action. On the other hand the nonlinear convective and pressure terms are much larger. (The pressure term is nonlinear through equation (6-3).) It may seem surprising that a small forcing term can produce large convective and pressure terms; apparently those terms are amplified by the instability of the Navier-Stokes flow at the Reynolds number in figure 6-4. The tendency is even greater at higher Reynolds numbers (not shown). If we compare the nonlinear convective and pressure terms with the viscous term rather than with the forcing term, the trend is not surprising, since it is well-known that the nonlinear terms become much greater than the viscous as the Reynolds number of a turbulent flow increases. As was mentioned before, the forcing term is of the same order of magnitude as the viscous.

Calculated spatial variations of velocity fluctuations are plotted in figure 6-6. Although the Reynolds number is low, there is some tendency for velocity gradients to become large in several nonadjacent regions, thus indicating the hydrodynamic instability of the flow and, in addition, the spatial intermittency of the flow in the smaller eddies (ref. 1). (Note that steep gradients are associated with small eddies or large wavenumbers (ref. 20).) This tendency to form steep gradients is, of course, a well-known property of turbulent flows, and evidently occurs as an effect of the nonlinear terms in the Navier-Stokes equations. In order to give an idea of the numerical resolution obtained, grid points are indicated by symbols; all of the scales of motion are well resolved.

The number of degrees of freedom or modes used in the present solution (32^3 grid points times three directional velocity components) was compared with the criteria for sufficient determining modes obtained by Constantin et al (ref. 11). Both on the basis of the ratio of the largest to smallest length scale and on the basis of Reynolds number, the number of determining modes used in the present solution was considerably larger than required for a *qual*itatively correct solution. So according to the criteria of reference 11, there are plenty of determining modes for a qualitatively correct solution. That reference does not address the problem of a *quan*titatively correct solution.

After initial transients have died out (for $t^* > 5$), the flow considered in figures 6-2 to 6-8 lies on a strange attractor. This is because, as shown in reference 9, the flow exhibits sensitive dependence on initial conditions, and because the Navier-Stokes equations represent a dissipative system, so that volumes in phase space, on the average, contract (for large times volumes in phase space approach zero!) (refs. 7, 8 and 21). We have also shown that sensitive dependence on initial conditions occurs for moderately high Reynolds-number decaying turbulence (ref. 22).

As a result of sensitive dependence on initial conditions it appears that one cannot obtain an analytical solution (at least in the usual sense), and we need not be apologetic about using a numerical solution for turbulent flows. Of course, one might use averaged, rather than instantaneous equations, but then the closure problem would appear (more unknowns than equations) (Chapt. IV), so that a deductive solution could not be obtained. (Averaged equations supposedly would not be chaotic.)

Figure 6-7 shows an instantaneous velocity vector field in the asymptotic (developed) region projected on the $x_1 - x_2$ plane through the numerical grid center. The time is $t^* = 13.28$. A few instantaneous streamlines have also been sketched in. The flow in figure 6-7 appears to be composed of randomly placed jets and whirls; other projections of the velocity vector field have a similar appearance, but with jets and whirls at different locations.

A three-dimensional representation of an instantaneous velocity field in the asymptotic region is given in figure 6-8. The magnitude of the velocity vector |u| is plotted on the $x_1 - x_2$ plane through the numerical grid center.

The time is again $t^* = 13.28$. Figure 6-8, as well as figure 6-7, illustrates the chaotic appearance of the velocity field. It is evident that the symmetry present in the nonrandom initial conditions in figures 6-2 and 6-3 has been broken for the developed flow in figures 6-7 and 6-8.

6.3 SOME COMPUTER ANIMATIONS OF A TURBULENT FLOW

Figures 6-2 to 6-8 give a good idea of the static appearance of the low Reynolds-number turbulent flow. In order to illustrate the dynamic evolution of the same flow, we have made some computer animations and put them on the Internet. They can be accessed via the Worldwide Web by visiting the following address: http://www.lerc.nasa.gov/WWW/GVIS/Deissler.html

In particular, the animation designated "Long-term solution for turbulent velocity" appears to give a perspective not readily obtained from a static representation.

6.4 SOME TURBULENT AND NONTURBULENT NAVIER-STOKES FLOWS

In this section (except for one of the flows considered for illustrative purposes in figure 6-9) we will use as initial conditions the spatially chaotic conditions in figures 6-7 and 6-8. These correspond to the flow in figure 6-4 at $t^* = 13.28$. As shown in reference 9, that flow is chaotic (the Liapunov characteristic exponent is positive). The use of chaotic initial conditions tends to assure that as many modes as possible are excited at a given Reynolds number. A chaotic initial condition, in fact, contains all modes; that is, it has a continuous spectrum.

The effectiveness of chaotic initial conditions in exciting unstable modes is illustrated in figure 6-9. The Reynolds numbers of both the *non*chaotic initial conditions and of the asymptotic flow in figure 6-9(a) are higher than those in figure 6-9(b), where the initial conditions are *chaotic*. Since the asymptotic flow in figure 6-9(a) is time-independent and that in figure 6-9(b) is chaotic, one sees that the character of these asymptotic flows is controlled by whether or not the initial conditions are chaotic, rather than by the Reynolds numbers. Of course if the initial Reynolds number is high enough, as in figure 6-4, the asymptotic flow may be chaotic even if the initial conditions are regular. At any rate it is clear from figure 6-9 that the use of chaotic initial conditions tends to make the asymptotic flow chaotic, when that is possible. It tends to insure that unstable modes are excited. But it will be seen that, depending on the final Reynolds number, a variety of asymptotic flows can be obtained from chaotic initial conditions.

The procedure for the calculations in the remainder of this section is this: The initial conditions, which are spatially chaotic, are obtained from the chaotic flow in figure 6-4 for $t^* = 13.28$. (See also figures 6-7 and 6-8.) Using that initial condition, the asymptotic Reynolds number for each flow is fixed by setting the value of χ in the forcing term in equation (6-4).

6.4.1 Time Series

Time series for seven different low Reynolds-number flows are shown in figures 6-10 and 6-4. In figure 6-10(a), where the asymptotic Reynolds number Re_a is 4.78 ($\chi = 0.2$), the asymptotic (long-time) flow is time-independent. This happens although the initial conditions are chaotic. Thus, the asymptotic Reynolds number here appears not to be high enough to sustain a time-dependent chaotic or periodic flow; no modes are active. In phase space this type of flow is a fixed point, as will be discussed in the next section.

For an asymptotic Reynolds number of 6.24 ($\chi = 0.3$) the longer-term solution (shown in fig. 6-10(b)) is periodic in time. The curve has a rather simple shape, although it is not as simple as a sine wave. As discussed in the next section, this is a limit cycle in phase space.

A more complicated periodic flow is plotted in figure 6-10(c), where the asymptotic Reynolds number has been increased to 6.67 ($\chi = 0.330$). The period is about twice that of the flow in figure 6-10(b). Thus, the solutions in figures 6-10(b) and (c) could be the first two members of a period-doubling sequence in a route to chaos (ref. 7). Further characterization of the flows in figures 6-10(b) and (c) will be given in the next section.

The asymptotic flow in figure 6-10(d), which is for a Reynolds number of 6.72 (($\chi = 0.338$), has some parts which appear to repeat, but it is not periodic. Even after a very long time we were unable to obtain a complete repeating cycle. In order to see if roundoff errors could produce that result, we increased those errors by several orders of

magnitude, but the results were unchanged. Figure 6-10(d) by itself does not provide enough information to satisfactorily characterize the flow in that figure. After we have calculated phase portraits, Poincaré sections, and Liapunov exponents, we will be in a better position to characterize the flow.

Consider next the asymptotic flow in figure 6-10(e), where the Reynolds number is 6.89 ($\chi = 0.35$). At first glance this flow might appear chaotic because of its complexity. It is, however, periodic, although the velocity variation within each period is quite complicated. This complex periodic flow has a period close to four times that of the simple periodic flow in figure 6-10(b). But it is not a third member of the period-doubling sequence of which the solutions in figures 6-10(b) and (c) appear to be the first two members. That is so because of the existence of the aperiodic flow in figure 6-10(d); it breaks up the sequence. Further discussion of the periodic flow in figure 6-10(e) will be given in following sections.

Finally, by increasing the asymptotic Reynolds number to 6.93 ($\chi = 0.4$) we get in figure 6-10(f) what appears to be a chaotic flow, since it has no apparent pattern. The flow has an appearance similar to that in figure 6-4 ($\chi = 1$) which was already shown to be chaotic (ref. 9).

In summarizing the information obtained from the time series for the various asymptotic flows, we note that the only flows that could be identified with reasonable certainty from the time series alone were the time-independent flow (fig. 6-10(a)) and the periodic flows in figures 6-10(b) and (e). We will be able to get a better understanding even of those flows from representations yet to be considered.

6.4.2 Phase Portraits

The term "phase portrait" as used here refers to a solution trajectory in the phase space of a flow. Since one cannot readily visualize a space of more than three dimensions, our representations will be projections of the higher-dimensional portraits onto two-dimensional planes or three-dimensional volumes in phase space.

The trajectory in figure 6-11(a), which corresponds to the time series in figure 6-10(a), shows an initial transient which ends at a stable fixed point in phase space. The arrow indicates the direction of increasing time (the direction of motion of the phase point). Since the velocity components at all points in physical space are time-independent for large times, the phase point occupies the same position in phase space for all large times. The projection in figure 6-11(a) is onto a $u_1(\pi,\pi,\pi) - u_2(\pi,\pi,\pi)$ plane; other projections are similar. This is the simplest example of an attractor, the trajectory in phase space being attracted to a single stable point. Once the phase point arrives there it does not leave. As mentioned earlier, volumes in phase space contract, on the average, in a dissipative system (refs. 7 and 21). In this case the volumes shrink down to a zero-volume zero-dimensional point. Motion in physical space does not of course cease but becomes time-independent.

Consider next the periodic phase portrait corresponding to the time series in figure 6-10(b) (see figs. 6-11(b) to (h)). Figures 6-11(b) and (c) show trajectories projected onto a $u_1(9\pi/8, 21\pi/16, 23\pi/16) - u_1(\pi,\pi,\pi)$ plane. Comparison of the unconverged orbit in figure 6-11(b) with the converged one in figure 6-11(c) shows that the unconverged curve wobbles around (on both sides of) the converged curve until it finally settles down on the latter. Thus, the trajectory is attracted to a stable limit cycle or periodic attractor. The fact that the phase point traces the same curve over and over (after convergence) confirms the periodicity of the orbit.

This formation of the stable limit cycle appears to be an example of order being born out of chaos (self-organization), since the flow was initially chaotic. For that to occur, it is only necessary to reduce the Reynolds number (or forcing) below its initial value by an appropriate amount.[3]

The contraction of volumes in phase space for a dissipative system again manifests itself here. Whereas in figure 6-11(a) the volumes shrink down to a zero-volume zero-dimensional point, for the periodic attractor considered here they shrink down to a zero-volume one-dimensional closed curve. The coordinate axis used to plot the curve will have the same shape as the curve itself. Thus, although the curve itself is one-dimensional, the one-dimensional coordinate system, or the basis function, may require many orthogonal dimensions to represent it. The curve is, strictly speaking, one-dimensional only when used with its own optimum one-dimensional coordinate system or basis function. Although the curve will not cross itself in its optimum coordinate system, it may cross when projected onto a two-dimensional orthogonal coordinate system (see fig. 6-11(d)).

[3]There may be an analogy here with the formation of the universe according to the presently accepted big-bang theory. According to that theory ordered structures (e.g., atoms, galaxies, stars, etc.) arose from an initial formless chaos (radiation). The structures could form when a parameter with an initially enormous magnitude, say the temperature, had decreased sufficiently. A nontechnical account of the theory is given in reference 23.

Additional projections of the periodic attractor onto planes in phase space are shown in figures 6-11(e) and (f) in order to give an idea of the variety of curve shapes that can be obtained. Note, that in figure 6-11(f), part of the symmetry present for t = 0 (fig. 6-2) has returned. (This symmetry is absent in the fully chaotic flows.) Projections of the orbit onto three-dimensional volumes in phase space are plotted in figures 6-11(g) and (h).

Projections of the period-two trajectory (corresponding to the time series in fig. 6-10(c) are plotted in figures 6-11(i) and (j). Comparison of those plots with the period-one plots in figures 6-11(c) and (d) shows that the single-cycle flow (with one large loop) has undergone a bifurcation to a two-cycle flow so that period doubling has occurred.

Phase-portrait projections corresponding to the time series in figure 6-10(d) are plotted in figures 6-11(k) to (q). This portrait differs qualitatively from the others shown so far, since it tends to fill a region of space in most of the two-dimensional projections. It was found that the longer the running time, the blacker is the portrait for the projections in figures 6-11(k) to (p). Thus, the trajectory is clearly not periodic, since if it were, it would be a closed curve in all projections. If it were quasiperiodic (with two independent frequencies), the phase portrait would lie on a torus. Figure 6-11(m) resembles a torus in some respects, but is more complicated. In particular, it has a knob in the central region.

The projections in figures 6-11(ℓ), (n), and (o) appear to show a sheet-like structure. Whereas for the periodic attractor of figures 6-11(c) to (h), phase-space volumes shrink down to a zero-volume line, here they appear to shrink down to a zero-volume sheet (or sheets). The notch in the projection in figure 6-11(n) is probably the result of a superposition of sheets. Sheet-like structures with folds are generic in strange attractors (ref. 7). Since in a chaotic flow there is stretching in at least one direction in phase space, there must be folding in order to keep the flow bounded. There appear to be some folds in the projections in figures 6-11(ℓ), (m), and (o), thus indicating that chaos is probable. The confused appearance of the trajectories in figures 6-11(k) and (p) is also indicative of chaos. Further evidence relative to the classification of this hard-to-classify flow will be considered in succeeding sections.

Projections of the periodic trajectory corresponding to the time series in figure 6-10(e) are plotted in figures 6-11(r) to (t). Initial transients have died out. Because of the very complicated appearance of the trajectory a cursory look might lead one to guess that it is chaotic (see also figure 6-10(e)). It is not chaotic, however, since it is not space filling. No matter how long a time the solution is continued, there is no blackening of the phase portrait; the same closed curve is traced over and over, indicating periodicity of the orbit. Since initial deviations or transients present in the flow (not shown) die out as the flow is attracted to a limiting curve, the long-term solution trajectory is a periodic attractor or limit cycle. The flow appears to have a remarkable memory in being able to repeat such a complicated orbit. The fact that such a complicated curve can be retraced is also indicative of the accuracy of the numerical method. As was the case for the simpler periodic attractors considered earlier, the present periodic attractor, although much more complicated, shows the shrinking of phase-space volumes to a zero volume one-dimensional curve. The discussion given there concerning the sense in which the curve is one-dimensional also applies here.

Increasing the Reynolds numbers to those in figures 6-10(f) and 6-4 we again get (as for figs. 6-11(k) to (o)) space-filling attractors. Projections of these are plotted in figures 6-11(u) to (x). After transients have died out, the trajectories are attracted to the black regions in the plots. These look like astrophysical black holes. Indeed, these attractors are similar to black holes in that for large times points cannot leave. A possible difference is that for somewhat earlier times, the phase points can cross over the attractors, leaving them momentarily. However that situation is temporary. After initial transients have completely died out, the phase points must remain forever on the attractors. These trajectories appear to be even more chaotic (have less of a pattern) than those in figures 6-11(k) to (o). However sheets and folding are less apparent than in the attractors for the lower Reynolds number in figures 6-11(k) to (o), probably because of the higher dimensionality of the attractors for the higher Reynolds numbers. More will be said about that in section 6.4.7.

6.4.3 Poincaré Sections

Poincaré sections are obtained by plotting the points where the phase point of a trajectory pierces (with increasing time) one side of a plane in phase space. The resulting plot has a dimension one less than that of the corresponding phase portrait. The lower-dimensional Poincaré section is sometimes easier to interpret. Here the pierced plane (Poincaré plane) is taken as a $u_1(\pi,\pi,\pi) - u_2(\pi,\pi,\pi)$ plane, and points are plotted when $u_1(9\pi/8, 21\pi/16, 23\pi/16)$

changes from positive to negative or from negative to positive. (Figure 6-11(g) may aid in visualizing the operation, at least for the simple periodic case).

For the fixed-point attractor in figure 6-11(a) a Poincaré section does not exist, except in a trivial sense, since the phase point does not pass through a plane as time increases. So we go on to the simple periodic attractor of figures 6-11(c) to (h). For that attractor the Poincaré sections are points. Figure 6-12(a) shows two Poincaré sections, one for u_1 ($9\pi/8$, $21\pi/16$, $23\pi/16$) changing from positive to negative and one for that coordinate changing from negative to positive as the phase point passes through a $u_1(\pi,\pi,\pi) - u_2(\pi,\pi,\pi)$ plane. (See also fig. 6-11(g) which plots the three coordinates.) Even after the phase point has pierced the Poincaré plane a large number of times (8 to 10), each section consists of a single point.

Consider next some Poincaré sections of the phase portrait for figures 6-11(k) to (q) ($\chi = 0.338$). These are plotted in figures 12(b) and (c). Some portions of the plots appear to be lines; that tends to indicate quasiperiodicity of the flow (with two independent frequencies). However, in other parts of the plots the points are scattered somewhat randomly with no apparent pattern; that tends to indicate chaos. Thus, the flow has both chaotic and quasiperiodic features. It is not periodic because longer running times produce more points on the Poincaré section.

Two Poincaré sections for the complex periodic attractor of figures 11(r) to (t) are plotted in figure 12(d). These sections are similar to those in figure 12(a), but because of the complexity of the attractor of figures 11(r) to (t), each section consists of five points instead of one. As was the case for the simpler periodic attractor, the number of points does not increase with increasing running time.

Finally, in figures 12(e) to (h), we consider Poincaré sections for our two highest Reynolds-number flows ($\chi = 0.4$ and 1). Phase portraits for these flows were considered in figures 11(u) to (x). These Poincaré sections are similar to those in figures 12(b) and (c) insofar as longer running times produce more plotted points. However they are qualitatively different, since there are no regions where the points lie along a curve. They tend to fill a region of space in an apparently random fashion; there is no evident pattern.

6.4.4 Liapunov Exponent

The Liapunov characteristic exponent (or largest Liapunov exponent if a spectrum of exponents is considered) provides a definitive way of determining whether or not a flow is chaotic. A positive Liapunov exponent indicates sensitive dependence on initial conditions, which in turn is often considered as synonymous with chaoticity.

The method used here to determine the sensitivity of our solutions to small changes in initial conditions, and to determine Liapunov exponents, is similar to one we used previously (ref. 9). The values of u_i at a time after initial transients have died out are perturbed by small spatially random numbers R, where $-10^{-6} < R < 10^{-6}$ or $-10^{-4} < R < 10^{-4}$. The perturbations are applied at each spatial grid point at one time. The distance between the perturbed and unperturbed solutions at various times is then calculated from

$$D = \left(\sum_{i,j} \left[u_{i,\text{perturbed}}(x_j, t) - u_{i,\text{unperturbed}}(x_j, t) \right]^2 \right)^{1/2} \qquad (6-9)$$

where i, which can have values from 1 to 3, indicates different directional velocity components, and j, which can go from 1 to some number M, indicates different points in physical space. Then D represents a distance or norm in a 3M-dimensional space. For M equal to the number of grid points, D is the distance in the phase space of the discretized system. (Note that the distance D has the dimensions of a velocity.)

In reference 9, D was represented by embedding it in one-, three-, six-, and twelve-dimensional space. It was found that increasing the embedding dimension from three to twelve had little or no effect on the calculated value of the Liapunov exponent. Here we adopt six dimensions as giving a sufficiently good representation of D. That is, we use three velocity components at each of two points in physical space as the dimensions (M = 2).

Thus, embedding the distance between perturbed and unperturbed solutions in a six-dimensional space and plotting $\log \left(D / \overline{u_0^2}^{1/2} \right)$ against dimensionless time, we obtain figures 13(a) to (c) for $\chi = 0.338$, 0.4, and 1. The values of log D, on the average, increase linearly with time, indicating that D increases exponentially. That is, initially neighboring solutions diverge exponentially on the average. Thus it appears that we can characterize these three flows as chaotic.

The fact that the mean slopes of the distance-evolution curves are constant over a considerable range also allows us to use our results to obtain an estimate of the Liapunov characteristic exponent. The Liapunov characteristic exponent σ (for times after initial transients have died out) is defined as (ref. 7)

$$\sigma = \lim_{\substack{t\to\infty \\ D(0)\to 0}} \left(\frac{1}{t}\right) \ln \frac{D(t)}{D(0)}, \tag{6-10}$$

where the D(t) are values of distance between initially neighboring solutions that might be obtained from figure 6-13. However, if the values of D were obtained from the wavy curves in figure 6-13, we would have to go to very large times in order to obtain a reasonable estimate for σ. This would take us out of the region of exponential growth of D, unless D(0) were very small (probably below the computer noise level). One way of getting around this difficulty is to use a renormalization procedure (ref. 7).

For our purposes it seems that, since the mean slopes of the distance evolution curves in figure 6-13 are constant over a considerable range, the best procedure is to replace the wavy curves by straight lines through them. Then equation (6-10) is replaced by

$$\sigma = \left[\ln\left(D_m/D_a\right)\right]/(t - t_a), \tag{6-11}$$

where the values of D_m and D_a are read from the straight line in each figure at times t and t_a, respectively. The straight line in each figure is drawn so that its mean square deviation from the wavy curve is a minimum; this procedure should give a good estimate for σ. The values of dimensionless σ so obtained for figures 6-13(a) to (c) are, respectively,

$$\left(x_0^2/\nu\right)\sigma \approx 0.12, \quad 0.35, \quad \text{and} \quad 2.7. \tag{6-12}$$

The value 2.7 agrees with that obtained for the same flow (but for a different time of perturbation and different embedding dimension) in reference 9. The Liapunov exponents in equation (6-12) give us a measure of the mean exponential rate of divergence of two initially neighboring solutions, or of the chaoticity of the flows. The important point is that σ is positive, indicating that these three flows are chaotic (ref. 7). It is noted that as the Reynolds number increases σ increases (for constant x_0 and ν), or the flows become more chaotic.

Plots of dimensionless D versus t* for our two periodic flows are given in figures 6-13(d) and (e). (Note two lost-data gaps in the figure 13(e) curve.) These plots are qualitatively different from those for chaotic flows. If they were not, of course, our method for calculating Liapunov exponents would be in error. Whereas D for chaotic flow increases exponentially (on the average) for about four orders of magnitude until it is of the same order as u_j, D for the periodic flows, on the average, shows no tendency to increase exponentially. Thus the Liapunov exponent does not show a tendency to be positive, as of course it should not, since the flow is not chaotic. Theoretically the largest Liapunov exponent, the one associated with perturbations along a trajectory, should be zero for a periodic attractor (ref. 24).

The following simple argument shows that the largest Liapunov exponent for a limit cycle is zero: A limit cycle is *stable*, so the flow must return to the same periodic attractor after a perturbation. That is, the trajectory, a long time after perturbation, must occupy the same points in phase space as it did before perturbation. So the only possible difference between the perturbed and unperturbed trajectories is that there may be a phase difference; although the trajectory, a long time after perturbation, must occupy the same points in phase space as does the unperturbed trajectory, it may do so at different times. A phase difference is allowable because our dynamical system is autonomous; time does not appear on the right side of equation (6-2). Since the velocity components are all periodic in time, D will be periodic, as in figure 6-13(f) and (g). There the limit cycle is perturbed along its trajectory by introducing a small phase difference Δt; the distance between neighboring solutions is calculated from

$$D_{phase} = \left(\sum_{i,j} \left[u_i\left(\mathbf{x}_j, t + \Delta t\right) - u_i\left(\mathbf{x}_j, t\right) \right]^2 \right)^{1/2} \tag{6-13}$$

in place of equation (6-9). Thus the average D over a long time has zero slope, so that for a periodic flow, the largest Liapunov exponent (associated with perturbations along the trajectory) is zero. Other Liapunov exponents (associated with perturbations normal to the trajectory) are negative, since the flow is attracted to the limit cycle. Note that figures 6-13(f) and (g) do not by themselves, without the rest of the above argument, show that the largest Liapunov exponent is zero. However the wavy curves in figures 6-13(d) and (e) do approach those in figures 6-13 (f) and (g) respectively for very long times. In particular the wavy-curve shape in figure 6-13(g) is nearly identical with that near the end of the curve in figure 13(e). So the use of equation (6-13) is a way of producing the asymptotic D's immediately when it is known that the asymptotic D's are the result of a phase difference, or of a perturbation along the trajectory. The effects of perturbations normal to the trajectory are absent in figures 13(f) and (g).

6.4.5 Ergodic Theory Interpretations

It may be worthwhile to look at our results in the light of modern ergodic theory (see refs. 7, 25, and section 4.1.1). According to that theory there is a hierarchy of random systems (fig. 6-14). At the bottom of the hierarchy are ergodic systems (those with equivalence of time, space, and ensemble averages); those systems embody the weakest notion of randomness. The so-called mixing systems (those that approach equilibrium) have a stronger notion of randomness than do those that are only ergodic, and systems that exhibit sensitive dependence on initial conditions, or chaoticity, have a stronger notion of randomness than do those that are only ergodic, or only ergodic and mixing. Mixing implies ergodicity, and chaoticity implies both ergodicity and mixing, but the converse is not true. At the top of the hierarchy are the most random systems; those that, though deterministic, may appear in a certain sense to behave as randomly as the numbers produced by a roulette wheel (Bernoulli systems) (ref. 25).

Recall that both of our flows show sensitive dependence on initial conditions (chaoticity), because of their positive Liapunov exponents. Thus, according to the hierarchy of randomness, they must both also be ergodic and mixing. The flow for the two higher asymptotic Reynolds numbers (Re_a = 6.93 and 13.3), in addition to being chaotic, mixing, and ergodic, have a Poincaré section without apparent pattern, in contrast to the lower Reynolds-number flow (Re_a = 6.72), where there was pattern in the Poincaré section. (Similar differences were observed in plots showing projections of the attractors for the two Reynolds numbers onto planes in phase space.) Thus the higher Reynolds-number flows have a higher degree of randomness than that required for chaoticity, and so are higher in the randomness hierarchy than is the lower Reynolds-number flow. That is, the higher Reynolds-number flows seem to have a stronger notion of randomness than chaoticity. In fact, the points on its Poincaré section appear to be placed about as randomly as the numbers produced by Roulette wheels.

For example, consider two Roulette wheels, one of which produces numbers corresponding to the abscissas of plotted points, and the other of which produces numbers corresponding to their ordinates. (Of course, one wheel could alternately be used for abscissas and ordinates). The plot so obtained from the spins of Roulette wheels would be similar to those in figures 12(e) to (h) (no apparent pattern), so that our higher Reynolds number flows may be close to a Bernoulli system. A possible explanation for the differences in the randomness exhibited by our two flows would be that the higher Reynolds-number flow has an attractor of higher dimension (>3) and thus a more confused (random) appearance.

6.3.5.1 Chaotic versus turbulent flows.—This leads us to a possible distinction between flows which are chaotic and those which, in addition, might be called turbulent. Perhaps one should reserve the term "turbulent" for flows which have both a positive Liapunov exponent and Poincaré sections without apparent pattern, as have those for Reynolds numbers Re_a of 6.93 and 13.3. Most flows called turbulent appear to be more random than required for a flow to be chaotic, although they are certainly chaotic, as well as ergodic and mixing.

Another characteristic which is often given as indicative of turbulence is a negative skewness factor S of the velocity derivative, where usually $-1 < S < 0$ (ref. 19). However, for the time-dependent flows considered here, both turbulent and nonturbulent, the skewness factor did not vary significantly from that given in equation (6-8). Even for the fixed-point flow (figs. 6-10(a) and 11(a)) the value of S was about –0.25. Thus although a negative S is necessary for the presence of turbulence, it is certainly not a sufficient indicator. A negative S in fact seems to be more an indicator of nonlinearity than of turbulence. All of the flows here are highly nonlinear.

6.4.6 Power Spectra

Power spectra give the distribution with frequency of the energy in a flow. We obtain the spectra by computing the fast Fourier transforms of the time series for the velocity components. The squares of the absolute values of those transforms are then plotted against dimensionless frequency. The results are given in figure 6-15.

Two types of spectra are indicated—discrete for the periodic flows and continuous for the chaotic ones. However, the spectra do not appear able to distinguish qualitatively between the weakly chaotic (fig. 6-15(b)) and the fully chaotic flows (figs. 6-15(d) and (e)). In that respect they are less sensitive indicators than are the Poincaré sections. If one considers the discrete and continuous spectra separately, then higher frequency components become excited as the Reynolds number increases (as χ increases). In the case of the discrete spectra, the simple periodic flow (fig. 6-15(a)) requires only four spectral components to represent u_2, whereas the much more complex periodic flow (fig. 6-15(c)) requires 36 nonnegligible components. In both cases the frequencies of the components are related to one another as ratios of integers (one fundamental frequency in each case).

6.4.7. Dimensions of the Attractors

As a final characterization of our Navier-Stokes flows, we consider the dimensions of the attractors on which the flows reside. The dimension of a space gives, in general, the number of quantities required to specify the position of a point in the space; e.g., one, two, or three coordinates are respectively required to specify a point in a one-, two-, or three-dimensional physical space. The same applies to an n-dimensional phase space, or to an attractor which is a portion of the phase space. The attractor is generally of lower dimension than that of the phase space because of the shrinking of volumes in the phase space of a dissipative system. It is partly this possibility of a decreased dimension of the attractor, and consequence simplification of the problem (in principle), which makes calculation of dimension an interesting pursuit. The dimension can be considered the lower bound on the number of essential variables needed to describe the dynamics of a system (ref. 26). Unfortunately it is usually difficult to obtain reliable estimates of that quantity.

As mentioned in section 6.4.2, the dimensions of our fixed-point and periodic attractors are respectively zero and one; a point in any space is zero-dimensional, and a closed curve, no matter how complicated its shape, is one-dimensional if the optimum coordinate system or basis function is used (see discussion in section 6.4.2).

One might question why more than one spectral component is required in figures 6-15(a) and (c) for the representation of one-dimensional periodic attractors. However the need for more than one component in those representations means only that the basis functions used there, sines and cosines, are not optimum for those cases. In the case of our complex periodic flow (fig. 6-15(c)) it would be necessary to use an extremely complicated basis function for one-spectral-component representation—most likely a basis function represented numerically rather than by an analytical function.

We also attempted to calculate the pointwise dimensions of our chaotic or strange attractors (refs. 26 and 27). In that attempt we have not been able to obtain a long enough time series for the dimension to become independent of time-series length. Thus, all we can say with certainty is that the dimension must be greater than 2; if it were not, trajectories for our chaotic flows would cross in phase space. They cannot cross for an autonomous system because if they did, there would be more than one trajectory for the same conditions (at the point where the trajectories cross), and the problem would not be deterministic.

One might expect that for our (weakly) chaotic flow the dimension would be only slightly greater than 2 because apparent folding can be seen in the phase portrait (figs. 11(ℓ) and (o)); if the attractor were many-dimensional, stretching and folding would occur in many directions and, because of the resulting confusion, could not be discerned in a two-dimensional plot. That is apparently what happens for the turbulent flows (figs. 11(u) to (x)). There the dimension must be significantly greater than 2; stretching and folding, although certainly present, is many-dimensional, so that the result is a confused appearance of the phase portrait. However, even there the dimension of the attractor should be limited by the overall shrinkage of volumes in phase space.

6.5 CONCLUDING REMARKS

Navier-Stokes turbulence is a chaotic phenomenon. Our long-term solutions with steady forcing show that the calculated turbulence has a positive Liapunov exponent, which in turn means that it is sensitively dependent on initial conditions.

Turbulence has, for a long time, been assumed to be random (ref. 1), or at least to have the appearance of randomness. Sensitive dependence on initial conditions provides an explanation for the occurrence of apparent randomness in turbulence. But in spite of its random appearance turbulence has a deterministic element, inasmuch as the Navier-Stokes equations which describe it are fully deterministic. The phrase "deterministic chaos" might therefore provide a fitting description for turbulence. Although turbulence is time-dependent and random in appearance, our solutions show that it can form with no time-dependent or random input. This again is a result of sensitive dependence of the solutions on initial conditions.

It may not, however, be a sufficiently complete description of turbulence to say that it is chaotic. Some of our low-Reynolds-number flows have a positive Liapunov exponent, and thus are chaotic, but their Poincaré sections show a pattern in some of their parts. On the other hand, solutions at somewhat higher Reynolds numbers show a complete lack of pattern. Perhaps we should reserve the term "turbulent" for flows that have a positive Liapunov exponent and, in addition, have Poincaré sections without pattern. Interpreting our results in the light of modern ergodic theory, turbulence is more random than required for a system to be chaotic; its randomness approaches that of a Bernoulli system, an example of which is a Roulette wheel.

Turbulence is also aperiodic or nonperiodic. As examples of flows which contrast with turbulence, we were able to obtain some periodic and fixed-point solutions. Whereas the fixed-point (in phase space) flows are time-independent, and the periodic flows are closed curves in phase space (points on Poincaré sections), the turbulent flows are time-dependent and fill a portion of phase space. The turbulent, periodic, and fixed-point flows are all attracted to lower-dimensional regions of phase space called attractors. The turbulent flows lie on strange or chaotic attractors.

Another requirement that is often given for flows to be turbulent is that they have negative velocity-derivative skewness factors. However, our periodic and fixed-point solutions have skewness factors that do not vary greatly from those for turbulent flows. A negative skewness factor seems to be more an indication of nonlinearity (all of our forced flows are highly nonlinear) than of turbulence.

APPENDIX I
CONTENTS OF RELATED TECHNICAL MEMORANDUMS

REFERENCES

1. Batchelor, G.K.: The Theory of Homogeneous Turbulence. Cambridge University Press, New York, 1953.
2. Herring, J.R.: An Introduction and Overview of Various Theoretical Approaches to Turbulence; in Theoretical Approaches to Turbulence, edited by D.L. Dwoyer, M.Y. Hussaini, and R.G. Voigt. Springer-Verlag, New York, 1985, pp. 73-90.
3. Kraichnan, R.H.: Decimated Amplitude Equations in Turbulence Dynamics; in Theoretical Approaches to Turbulence, edited by D.L. Dwoyer, M.Y. Hussaini, and R.G. Voigt. Springer-Verlag, New York, 1985, pp. 91–136.
4. Deissler, R.G.: Turbulence Processes and Simple Closure Schemes; in Handbook of Turbulence, edited by W. Frost and T.H. Moulden. Plenum Press, New York, 1977, vol. I, pp. 165–186.
5. Lin, C.C.; and Reid, W.H.: Turbulent Flow, Theoretical Aspects; in Handbuch der Physik, edited by S. Flügge, and Truesdell, C. Springer-Verlag, New York, 1963, vol. VIII/2.
6. Ruelle, D.; and Takens, F.: On the Nature of Turbulence. Commun. Math. Phys. vol. 20(3), pp. 167–192 (1971).
7. Lichtenberg, A.J.; and Lieberman, M.A.: Regular and Stochastic Motion. Springer-Verlag, New York, 1983.
8. Deissler, R.G.: Turbulent Solutions of the Equations of Fluid Motion. Rev. Mod. Phys. vol. 56, pp. 223–254 (1984).
9. Deissler, R.G.: Is Navier-Stokes Turbulence Chaotic? Phys. Fluids, vol. 29, pp. 1453–1457 (1986).
10. Deissler, R.J.: External Noise and the Origin and Dynamics of Structure in Convectively Unstable Systems, J. Stat. Phys. vol. 54 (5/6), pp. 1459–1488 (1989).
11. Constantin, P.; Foias, C.,; Manley, O.P., and Teman, R.: Determining Modes and Fractal Dimension of Turbulent Flows. J. Fluid Mech. vol. 150, pp. 427–440 (1985).
12. Lorenz, E.N.: Deterministic Nonperiodic Flow. J. Atmos. Sci., vol. 20, 1963, pp. 130–141.
13. Landau, L.D.: On the Problem of Turbulence. C.R. Acad. Sci. USSR, vol. 44, 1944, p. 311 (also in Collected Papers of Landau, ed by D. ter Haar, p. 387).
14. Landau, L.D.; and Lifshitz, E.M.: Fluid Mechanics, Chapter III. Pergamon Press, New York, 1959.
15. Deissler, R.G.: Nonlinear Decay of a Disturbance in an Unbounded Viscous Fluid. NASA TN D–4947, 1968. (Also in Appl. Sci. Res., vol. 21, no. 6, Jan. 1970, pp. 393–410).
16. Goldstein, M.E.; and Braun, W.H.: Advanced Methods for the Solution of Differential Equations. NASA SP–316, 1973.
17. Deissler, R.G.: On the Nature of Navier-Stokes Turbulence. NASA TM–101983, 1989. (Also in Encyclopedia of Fluid Mechanics, Supplement 1, Applid Mathematics in Fluid Dynamics, Ed. by N.P. Cheremisinoff. Gulf Publ. Co., Houston, 1993, pp. 1–51.)
18. Clark, R.A.; Ferziger, J.H.; and Reynolds, W.C.: Evaluation of Subgrid-Scale Models Using an Accurately Simulated Turbulent Flow. J. Fluid Mech. vol. 91, pp. 1–16, (1979).
19. Tavoularis, S.; Bennett, J.C.; and Corrsin, S.: Velocity-Derivative Skewness in Small Reynolds Number, Nearly Isotropic Turbulence. J. Fluid Mech., vol. 88, 1978, pp. 63–69.
20. Sokolnikoff, I.S.: Advanced Calculus, McGraw-Hill Book Co., New York, 1939, pp. 391, 392, fig. 83.
21. Constantin, P.; Foias, C.; and Temam, R.: Attractors Representing Turbulent Flows. Memoirs, Amer. Math. Soc., vol. 53, no. 314, 1985, p. 57.
22. Deissler, R.G.; and Molls, F.B.: Effect of Spatial Resolution on Apparent Sensitivity to Initial Conditions of a Decaying Flow as it Becomes Turbulent. J. Comp. Phys., vol. 100, no. 2, June, 1992, pp. 430–432.
23. Jastrow, R.: God and the Astronomers. W.W. Norton, New York, 1978.
24. Haken, H.: Advanced Synergetics. Springer-Verlag, New York, 1983.
25. Lebowitz, J.L.; and Penrose, O.: Modern Ergodic Theory. Phys. Today vol. 26, no. 2, 1973, pp. 23–29.
26. Farmer, J.D.; Ott, E.; and Yorke, J.A.: The Dimension of Chaotic Attractors. Physica D, vol. 7D, 1983, pp. 153–180.
27. Guckenheimer, J.; and Buzyna, G.: Dimension Measurements for Geostrophic Turbulnece. Phys. Rev. Lett., vol. 51, no. 16, 1983, pp. 1438–1441.

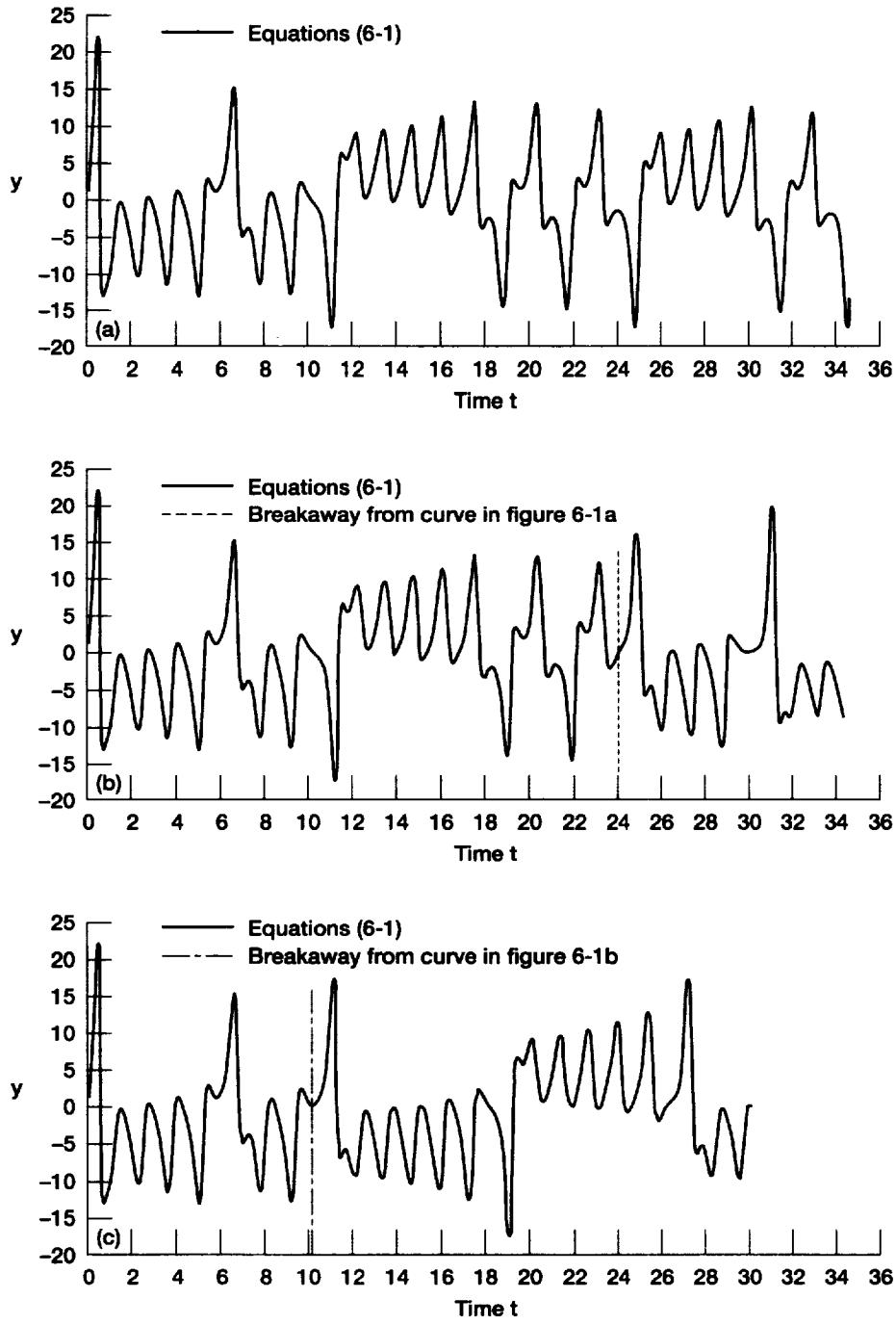

Figure 6-1.—Evolution of the mode y in the three-mode Lorenz system (eqs. (6-1)). Solution obtained numerically by improved Euler method. b = 1, r = 26, s = 3, initial x = initial z = 0. (a) Initial y = 1.000, Δt in numerical solution = 0.002. (b) Initial y = 1.001, Δt in numerical solution = 0.002. (c) Initial y = 1.001, Δt in numerical solution = 0.01.

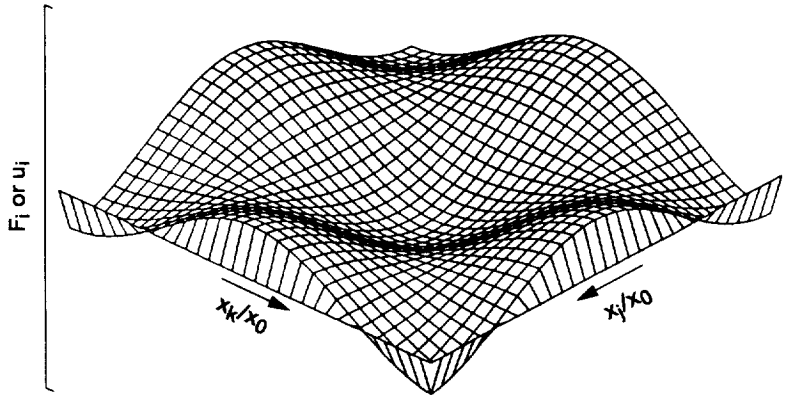

Figure 6-2.— Plot of forcing term F_i in equation (6-2) or of regular initial velocity component u_i on a plane through center of numerical grid. x_k and x_j are coordinates on the plane and x_0 is the reciprocal of a wave-number component of the forcing term.

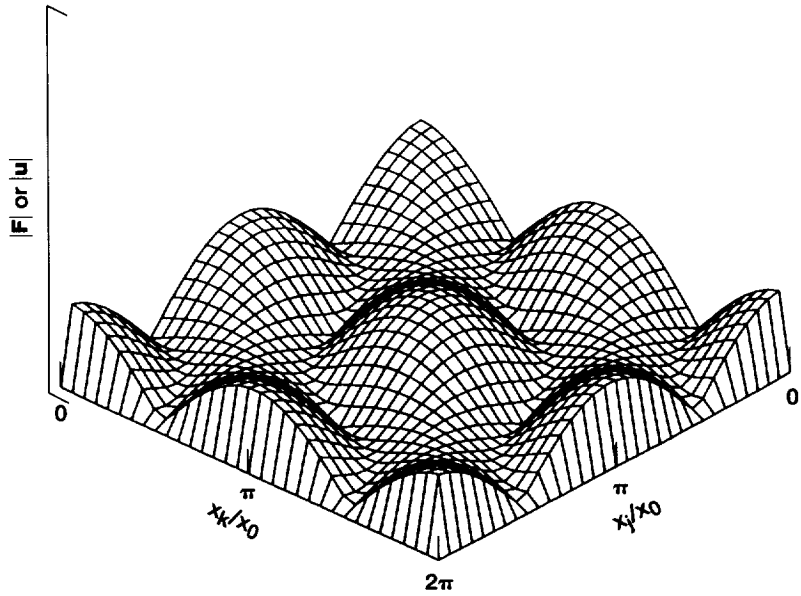

Figure 6-3.—Magnitude of forcing vector or of regular initial velocity vector on a plane through numerical-grid center.

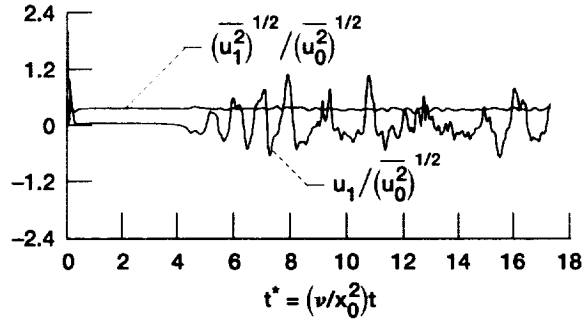

Figure 6-4.—Calculated evolution of turbulent velocity fluctuations with a time-independent forcing term. Ordinates normalized by initial condition. Root-mean square velocities (with a single bar) are spatially averaged. Developed Reynolds number $\overline{\overline{(u_1^2)}}^{1/2}\, x_0/\nu = 13.3$, where the double bar indicates an average over space and time for $t^* > 5$, $\chi = 1$. $x_1^* = x_1/x_0 = 9\pi/8$, $x_2^* = 21\pi/16$, $x_3^* = 23\pi/16$, for unaveraged fluctuations. 32^3 spatial grid points.

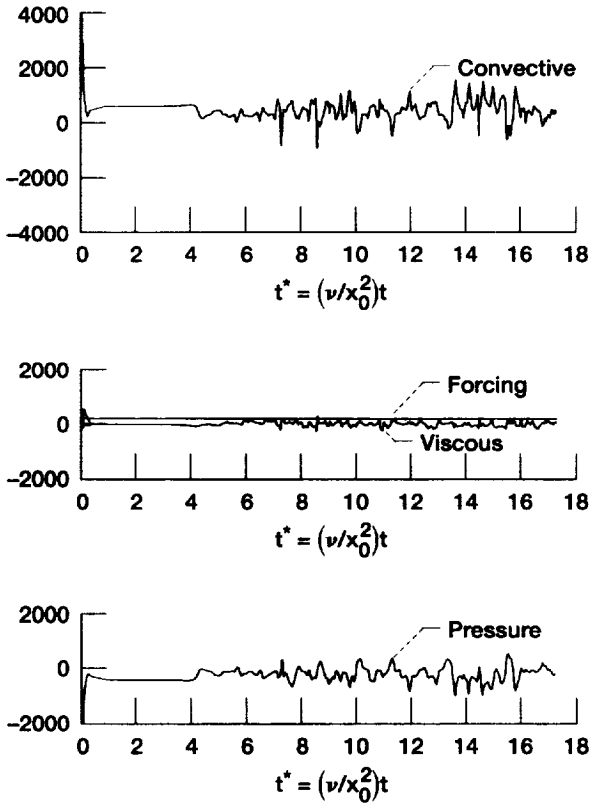

Figure 6-5.—Calculated evolution of instantaneous terms in Navier-Stokes equation at grid center. $\chi = 1$. Developed Reynolds number = 13.3.

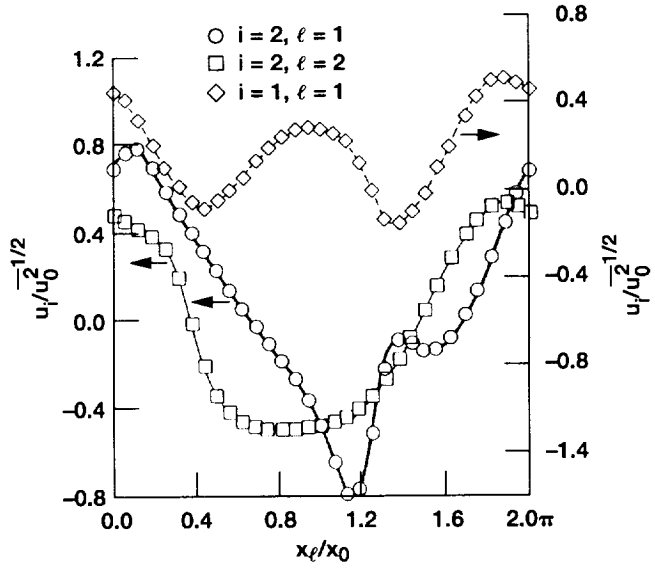

Figure 6-6.—Calculated spatial variation of velocity fluctuations on a plane through grid center at t* = 13.74. Symbols are at grid points.

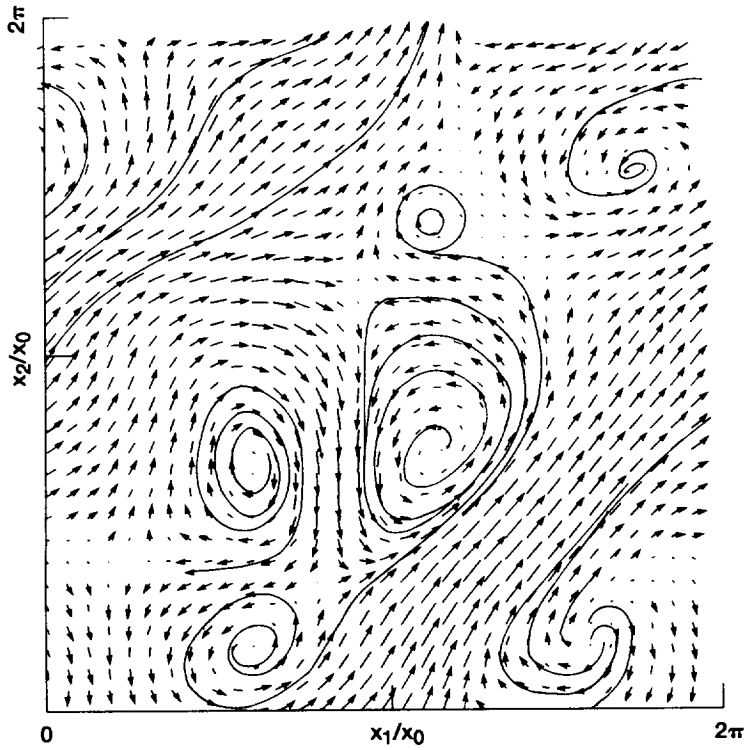

Figure 6-7.—Plot of projection of velocity-vector field on $x_1 - x_2$ plane through grid center. Lengths of arrows are proportional to velocity magnitudes. Also shown are some streamlines. $\chi = 1$. t* = 13.28.

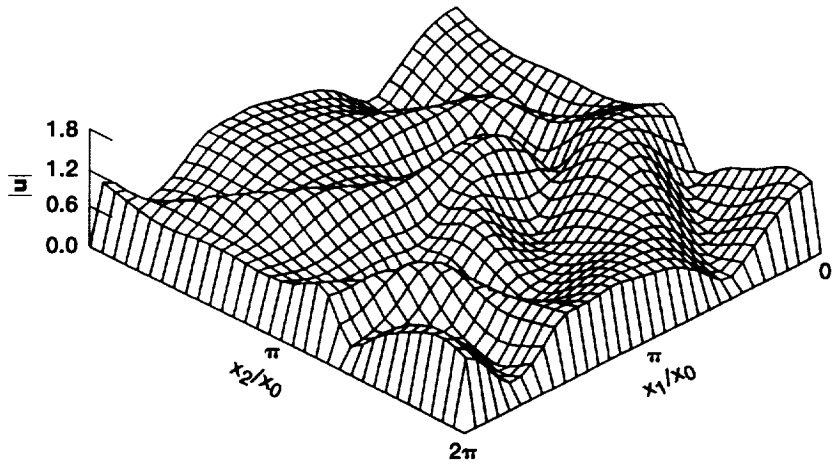

Figure 6-8.—Magnitude of spatially chaotic initial velocity vector on plane through grid center. $t^* = 13.28$.

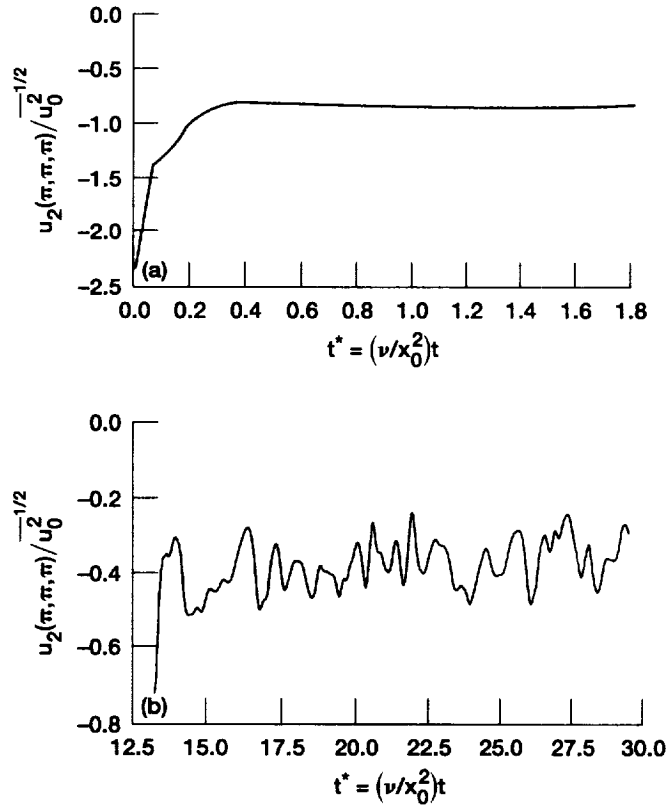

Figure 6-9.—Effects of type of initial flow and of Reynolds number on asymptotic flow. (a) Initial flow, regular. Initial Reynolds number = 17.3. Asymptotic Reynolds number = 8.5. (b) Initial flow, chaotic. Initial Reynolds number = 13.3. Asymptotic Reynolds number = 7.4.

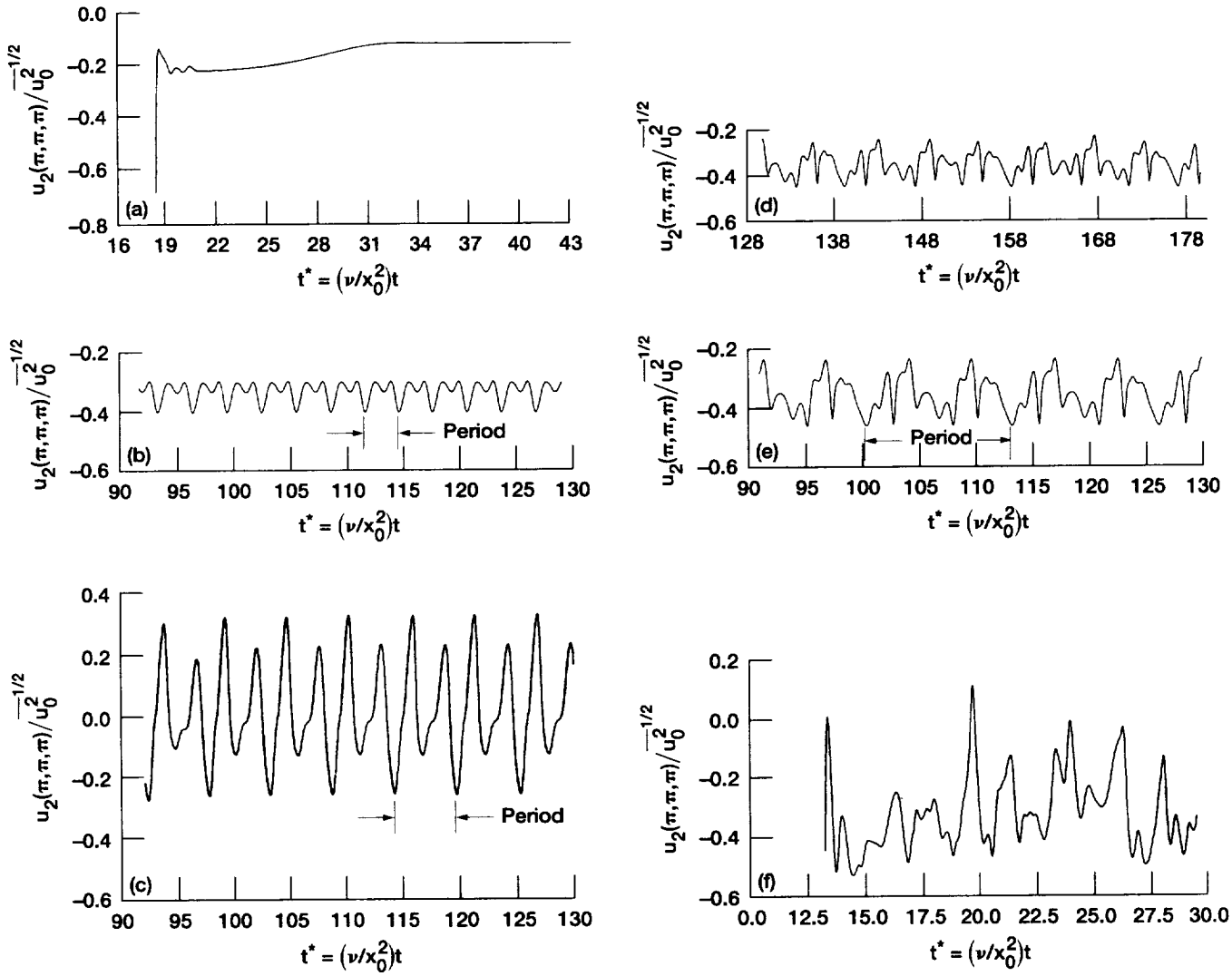

Figure 6-10.—Calculated time series for evolution of velocity component. Initial flow, chaotic. Initial Reynolds number = 13.3. (a) Asymptotic Reynolds number $Re_a = 4.78$ or $\chi = 0.2$. Fixed-point flow. (b) $Re_a = 6.24$ or $\chi = 0.3$. Simple periodic flow. (c) $Re_a = 6.67$ or $\chi = 0.330$. Period-two flow. (d) $Re_a = 6.72$ or $\chi = 0.338$. (e) $Re_a = 6.88$ or $\chi = 0.35$. Complex periodic flow. (f) $Re_a = 6.93$ or $\chi = 0.4$.

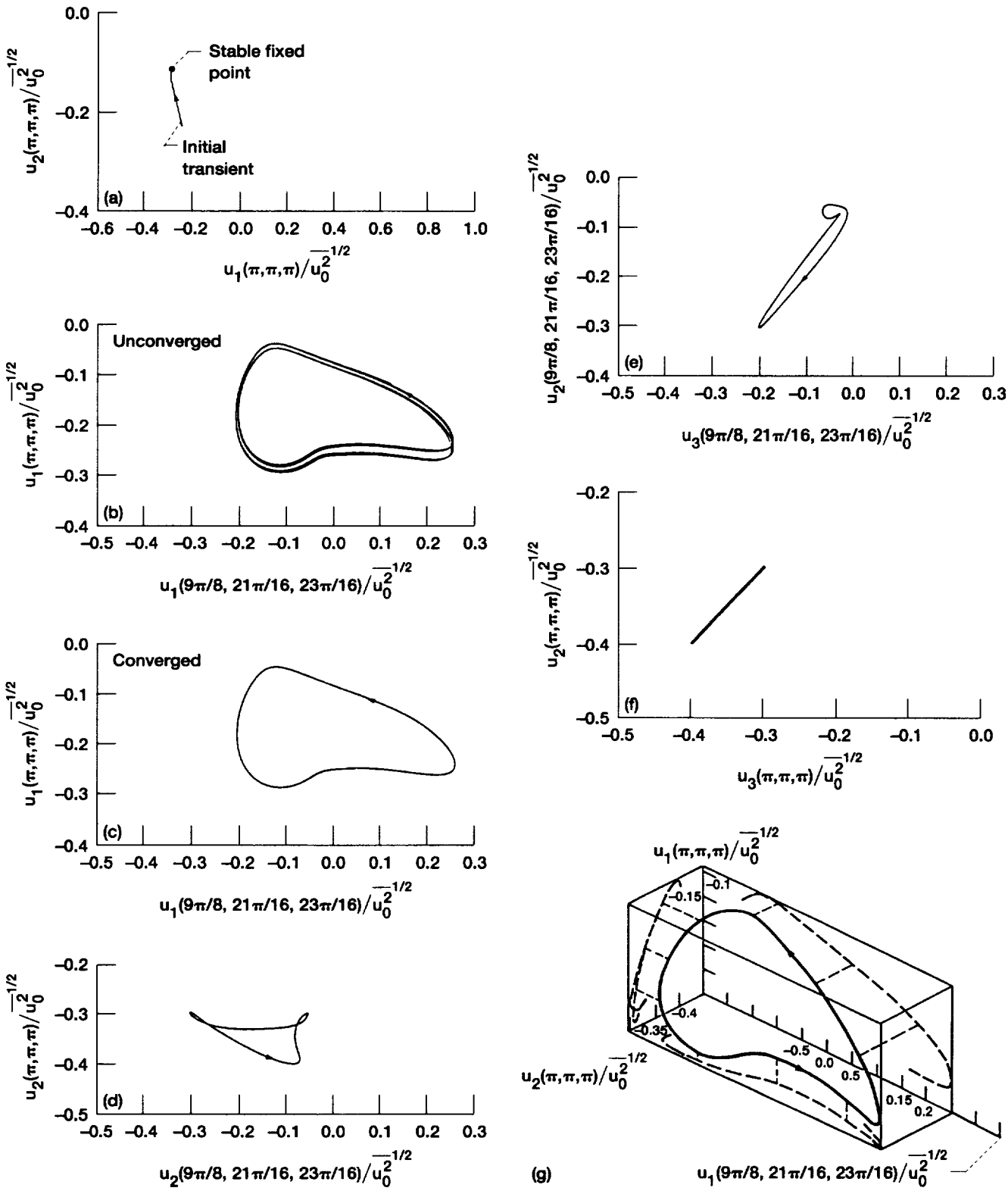

Figure 6-11.—Projected phase portraits. (a) Re_a = 4.78 or χ = 0.2. Transient and fixed point flow. $t^* > 21$. (b) Re_a = 6.24 or χ = 0.3. Simple periodic flow. (c) Re_a = 6.24 or χ = 0.3. (d) Re_a = 6.24 or χ = 0.3. (e) Re_a = 6.24 or χ = 0.3. Simple periodic flow. (f) Re_a = 6.24 or χ = 0.3. (g) Re_a = 6.24 or χ = 0.3.

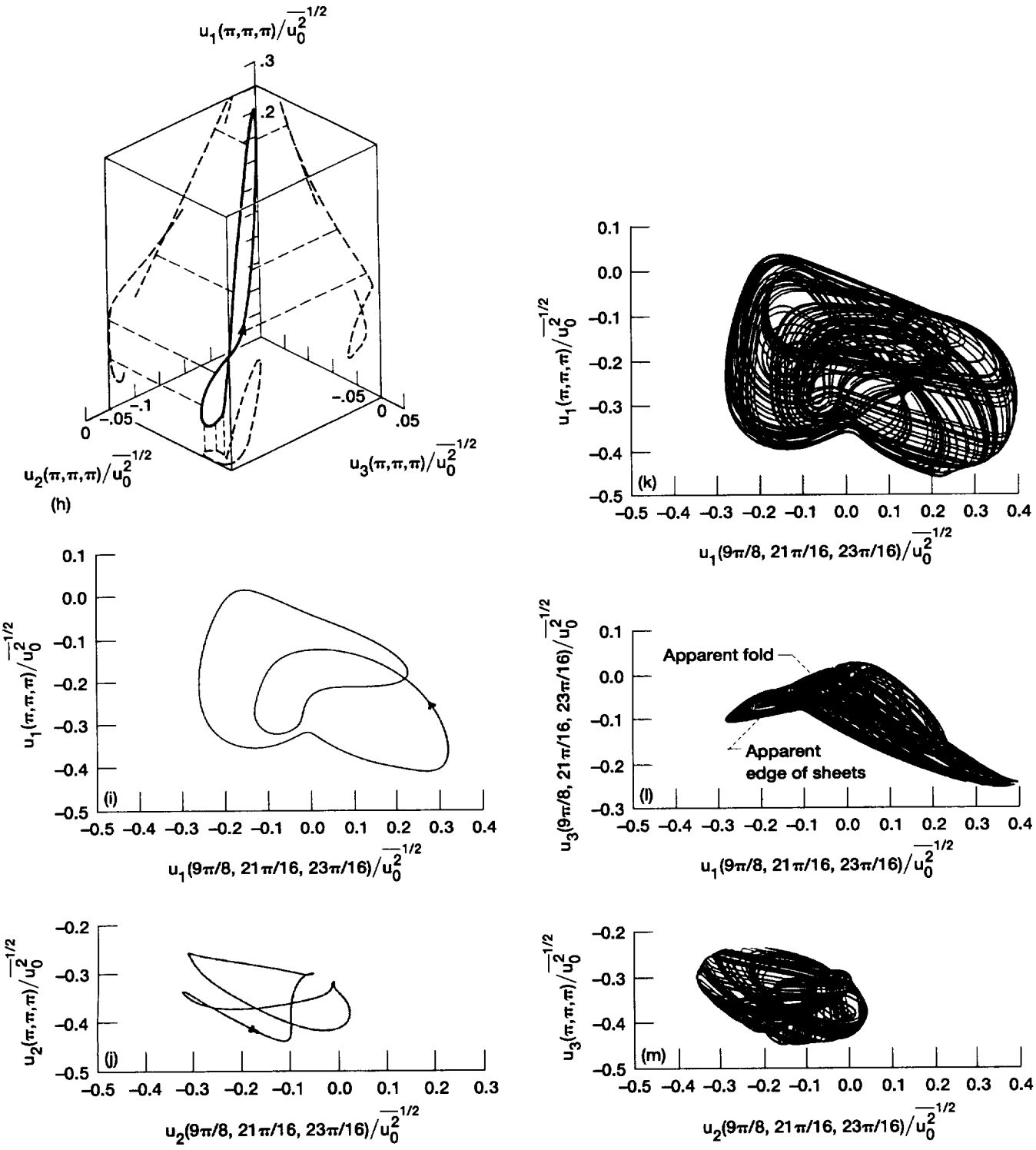

Figure 6-11.—Continued. (h) $Re_a = 6.24$ or $\chi = 0.3$. Simple periodic flow. (i) $Re_a = 6.67$ or $\chi = 0.330$. Period-two flow. (j) $Re_a = 6.67$ or $\chi = 0.330$. Period-two flow. (k) $Re_a = 6.72$ or $\chi = 0.338$. (l) $Re_a = 6.72$ or $\chi = 0.338$. (m) $Re_a = 6.72$ or $\chi = 0.338$.

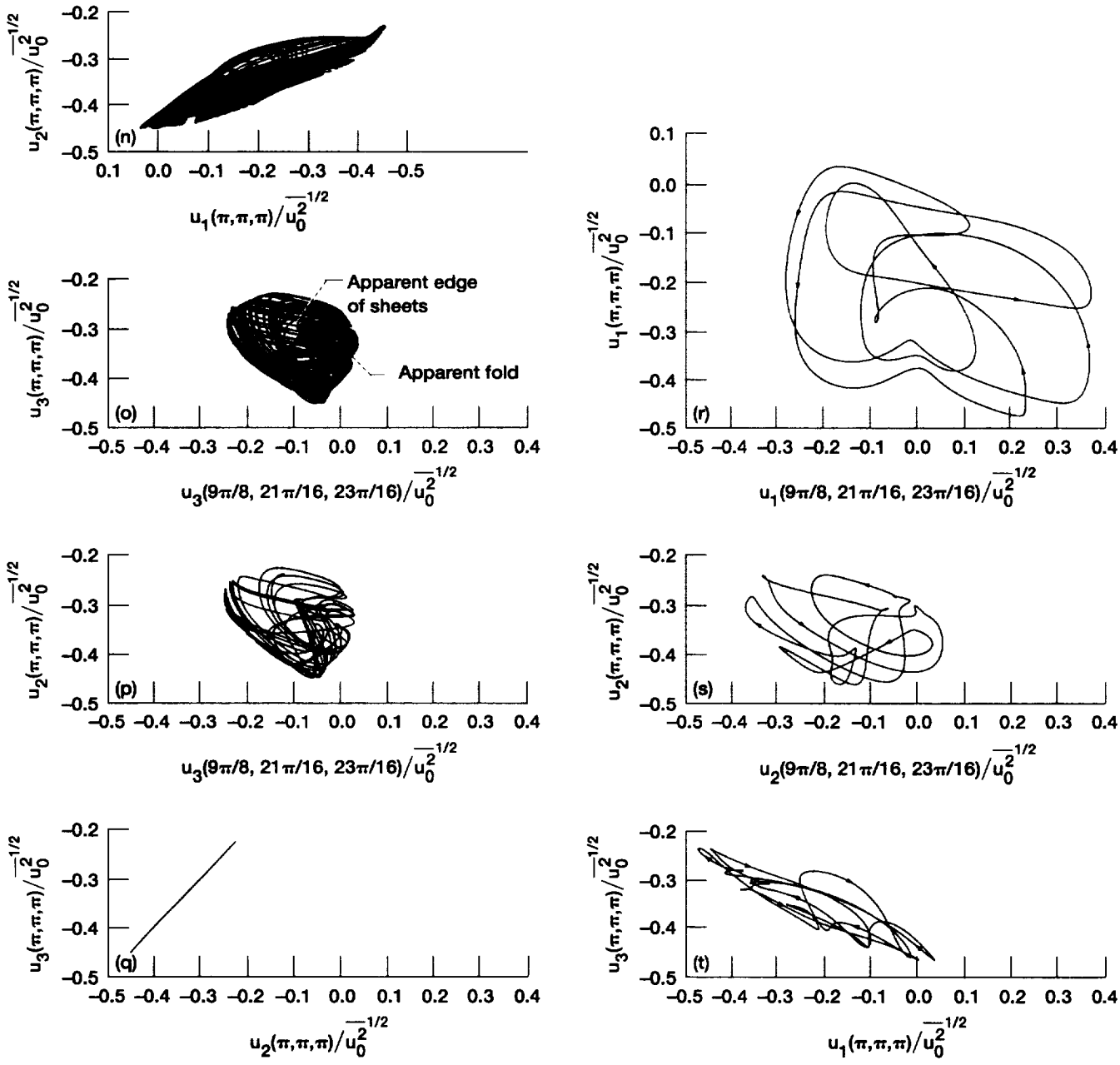

Figure 6-11.—Continued. (n) Re_a = 6.72 or χ = 0.338. (o) Re_a = 6.72 or χ = 0.338. (p) Re_a = 6.72 or χ = 0.338. (q) Re_a = 6.72 or χ = 0.338. (r) Re_a = 6.88 or χ = 0.35. (s) Re_a = 6.88 or χ = 0.35. (t) Re_a = 6.88 or χ = 0.35.

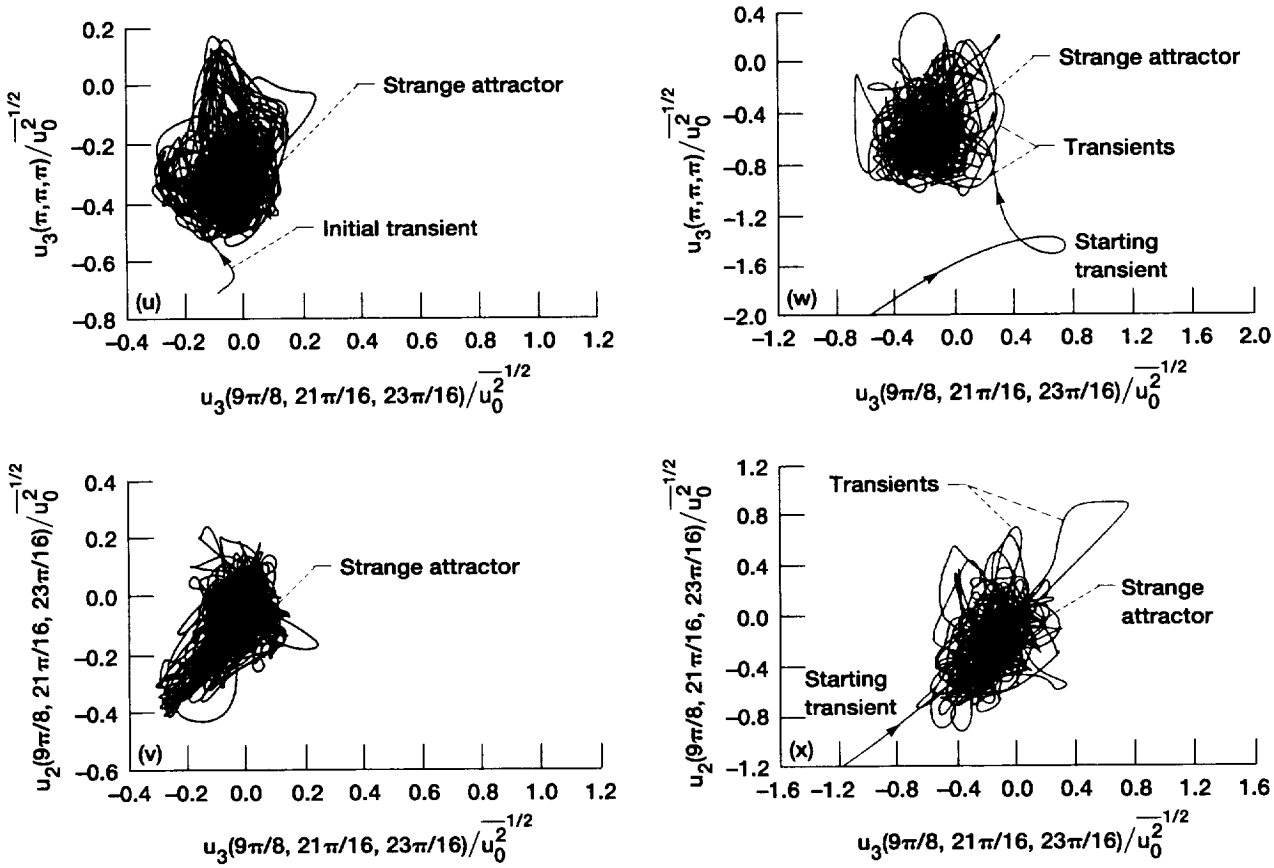

Figure 6-11.—Concluded. (u) Re_a = 6.93 or χ = 0.4. (v) Re_a = 6.93 or χ = 0.4. (w) Re_a = 13.3 or χ = 1. (x) Re_a = 13.3 or χ = 1.

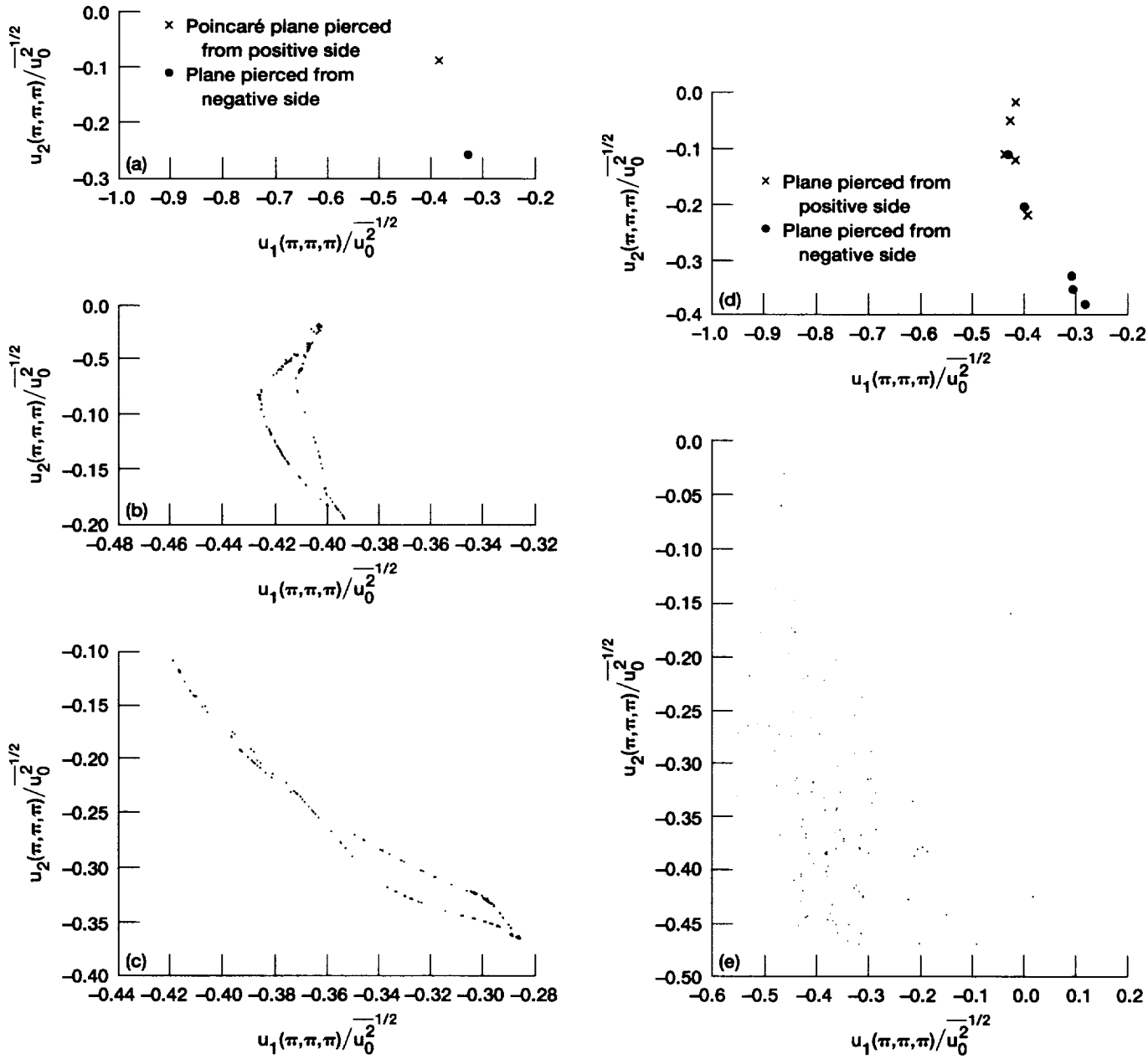

Figure 6-12.—Poincaré sections of attractors. (a) Re_a = 6.24 or χ = 0.3. Simple periodic flow. (b) Plane pierced from positive side, Re_a = 6.72 or χ = 0.338. (c) Plane pierced from negative side, Re_a = 6.72 or χ = 0.338. (d) Re_a = 6.88 or χ = 0.35. Complex periodic flow. (e) Plane pierced from negative side. Re_a = 6.93 or χ = 0.4.

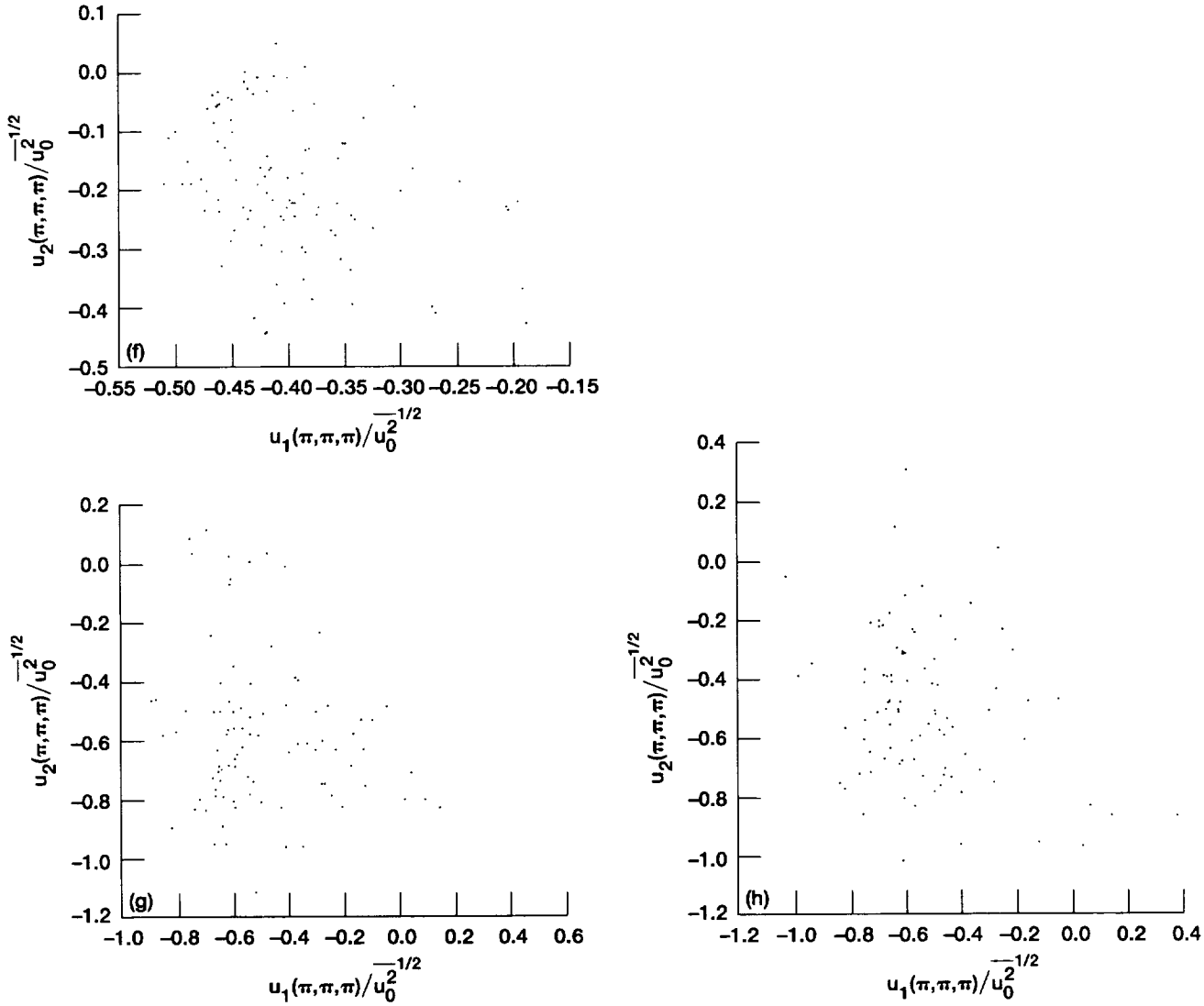

Figure 6-12.—Concluded. (f) Plane pierced from positive side. Re_a = 6.93 or χ = 0.4. (g) Plane pierced from negative side. Re_a = 13.3 or χ = 1. (h) Plane pierced from positive side. Re_a = 13.3 or χ = 1.

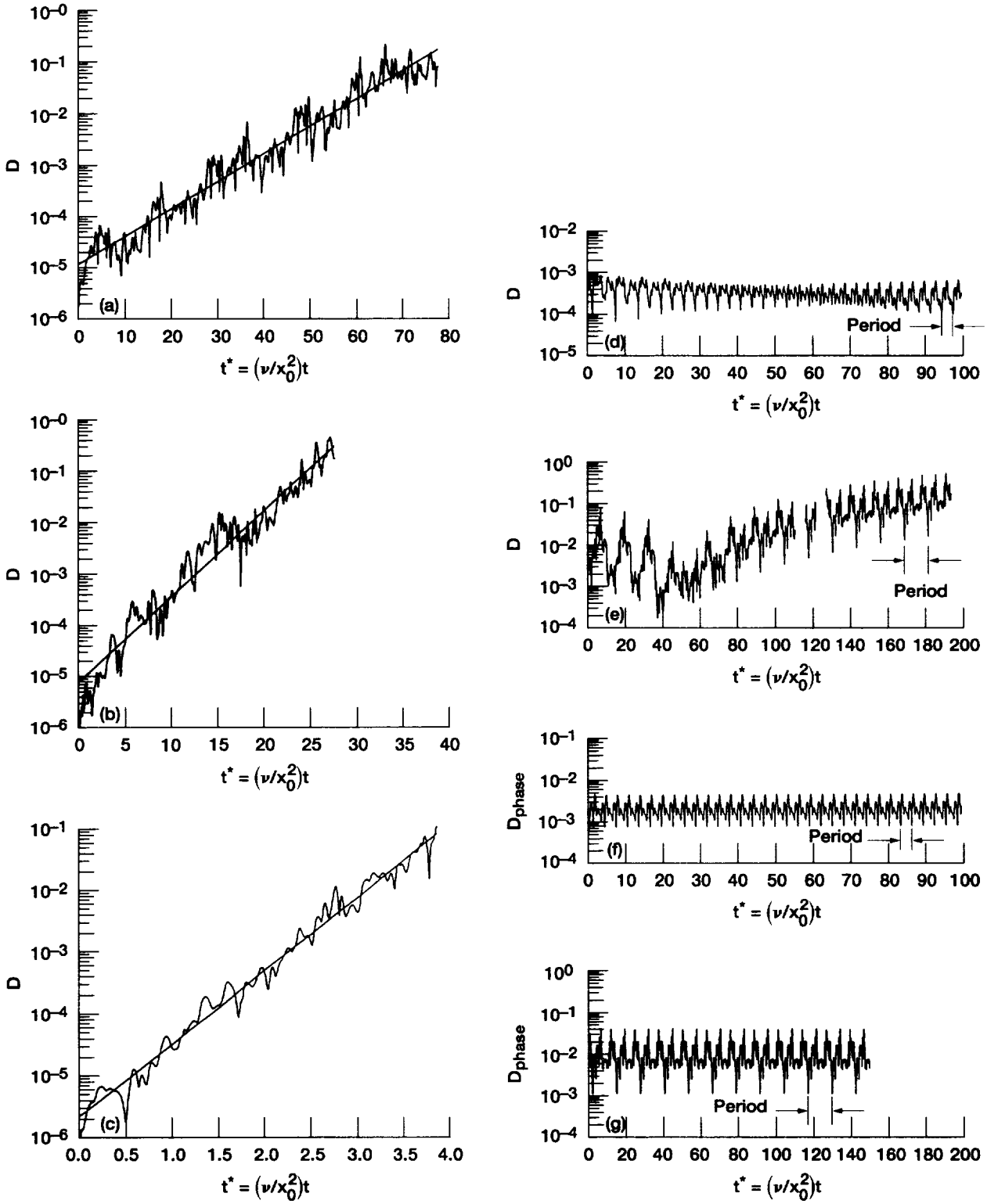

Figure 6-13.—Semilogarithmic plots showing evolution of distance D between initially neighboring solutions. (a) $Re_a = 6.72$ or $\chi = 0.338$. $-10^{-6} < R < 10^{-6}$. Chaotic flow. (b) $Re_a = 6.93$ or $\chi = 0.4$. $-10^{-6} < R < 10^{-6}$. Chaotic flow. (c) $Re_a = 13.3$ or $\chi = 1$. $-10^{-6} < R < 10^{-6}$. Chaotic flow. (d) $Re_a = 6.24$ or $\chi = 0.3$. $-10^{-4} < R < 10^{-4}$. Simple periodic flow. (e) $Re_a = 6.88$ or $\chi = 0.35$. Complex periodic flow. (f) Separation distance if phase point is perturbed only along trajectory. $Re_a = 6.24$ or $\chi = 0.3$. Simple periodic flow. (g) Separation distance if phase point is perturbed only along trajectory. $Re_a = 6.88$ or $\chi = 0.35$. Complex periodic flow.

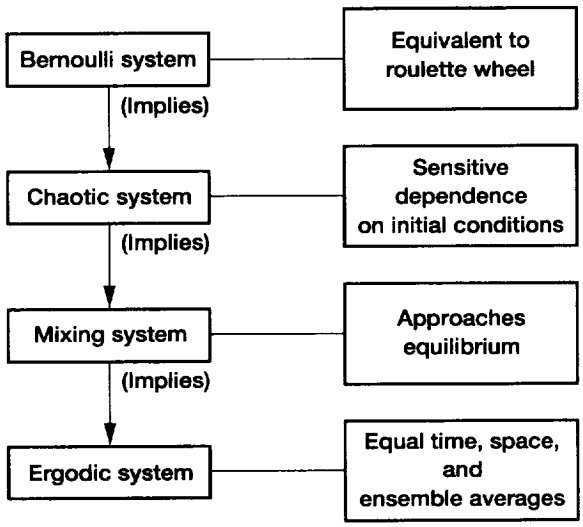

Figure 6-14.—Randomness hierarchy.

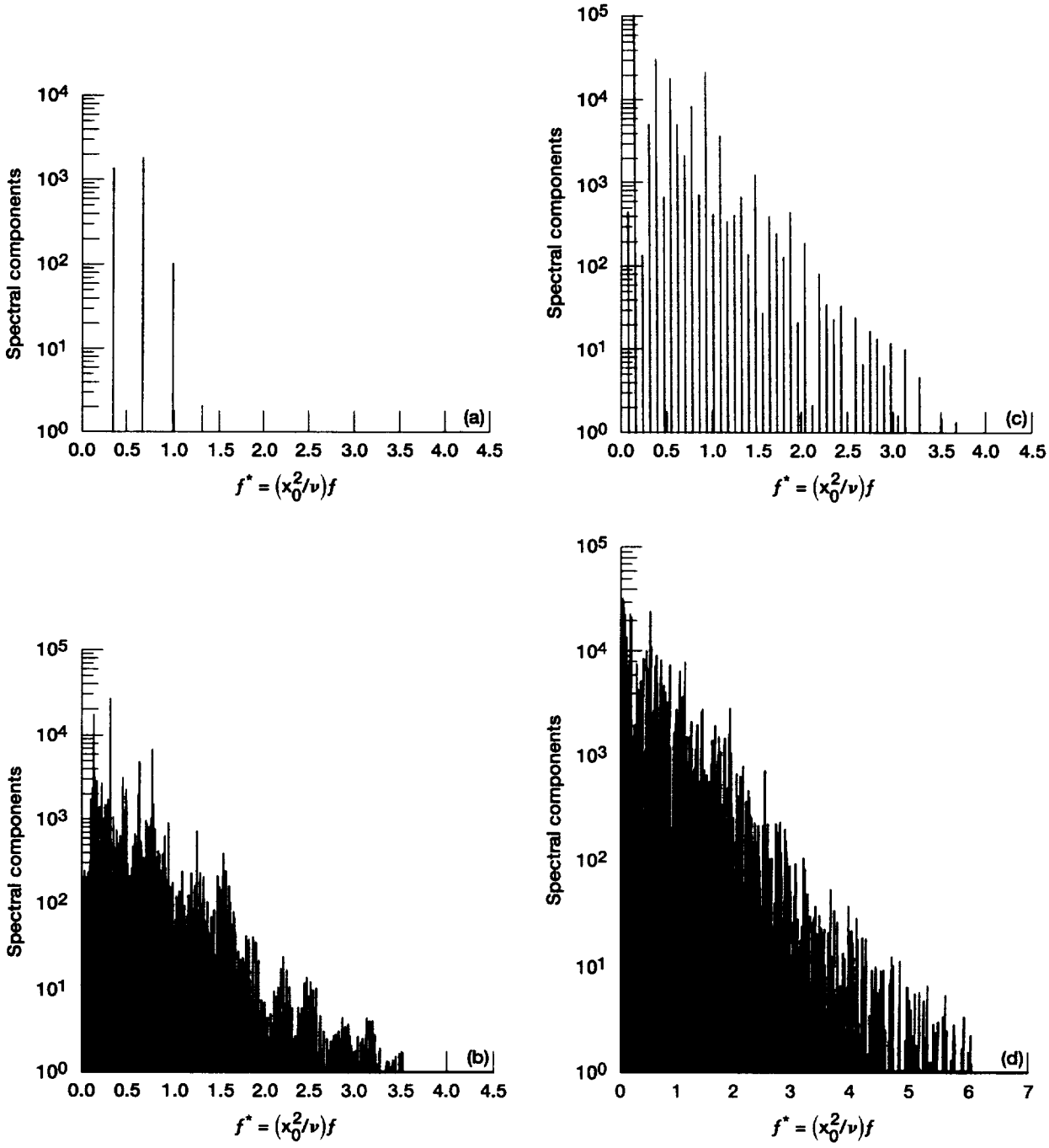

Figure 6-15.—Power Spectra of $u_2(\pi,\pi,\pi)/\overline{u_0^2}^{1/2}$. (a) Re_a = 6.24 or χ = 0.3. Simple periodic flow. (b) Re_a = 6.72 or χ = 0.338. Weakly chaotic flow. (c) Re_a = 6.88 or χ = 0.35. Complex periodic flow. (d) Re_a = 6.93 or χ = 0.4. Chaotic flow.

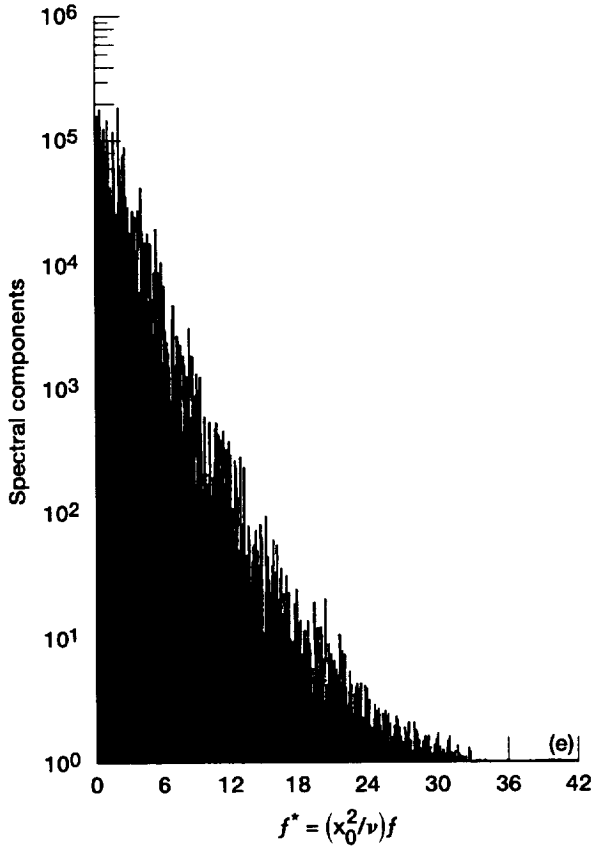

Figure 6-15.—Concluded. (e) Re_a = 13.3 or χ = 1. Chaotic flow.

EPILOGUE

Advances in solving the turbulence problem continue to be made along theoretical, computational, and experimental lines. Considerable progress in understanding turbulence mechanisms, particularly spectral energy transfer and the interaction between energy transfer and dissipation, has been made by using theoretical and computational methods. Much of the recent activity in turbulence research is related to advances in high-speed computation. For example, deductive-computational solutions of the unaveraged Navier-Stokes equations are now available, at least for turbulent flows at low and moderate Reynolds numbers. A Reynolds number higher than those which can be handled by available computers and computational schemes can, of course, always be picked. However, at least from a research standpoint, high Reynolds-number turbulence does not differ qualitatively from that at lower Reynolds numbers; the turbulent energy is just spread out over a wider range of wavenumbers, there being no bifurcations in going from low to high Reynolds numbers except possibly in the transition region between laminar and turbulent flow. The mathematical and computational methods appropriate for low and for high Reynolds numbers may of course differ.

Another area of progress is in the application of nonlinear-dynamics and chaos theory to turbulence research. Here again the research could not get very far without the use of high-speed computation. Nonlinear-dynamics and chaos theory has given us a means of interpreting numerical results by providing new investigative tools. Turbulence, while chaotic, is shown to be more random than is required for a chaotic flow.

From an engineering standpoint quantitative results at high Reynolds numbers are required. There, modeling, or the use of information in addition to that provided by the Navier-Stokes equations still has a place in turbulence calculations.

Advances in solving the turbulence problem will no doubt continue. For example, faster computers should become available and make possible turbulent solutions of the unaveraged Navier-Stokes equations at higher Reynolds numbers; those solutions could then be interpreted by the use of nonlinear-dynamics and chaos theory. At the same time advances in the use of modeling in the solution of the averaged Navier-Stokes equations should give engineering results at possibly still higher Reynolds numbers. Eventually, as still faster computers become available, results from the two approaches (deductive-computational and modeling) will hopefully merge.

REPORT DOCUMENTATION PAGE

Form Approved
OMB No. 0704-0188

1. AGENCY USE ONLY (*Leave blank*)	2. REPORT DATE	3. REPORT TYPE AND DATES COVERED
	September 1996	Technical Memorandum

4. TITLE AND SUBTITLE

Turbulent Fluid Motion VI—
Turbulence, Nonlinear Dynamics, and Deterministic Chaos

5. FUNDING NUMBERS

WU–505–90–53

6. AUTHOR(S)

Robert G. Deissler

7. PERFORMING ORGANIZATION NAME(S) AND ADDRESS(ES)

National Aeronautics and Space Administration
Lewis Research Center
Cleveland, Ohio 44135–3191

8. PERFORMING ORGANIZATION REPORT NUMBER

E–9845

9. SPONSORING/MONITORING AGENCY NAME(S) AND ADDRESS(ES)

National Aeronautics and Space Administration
Washington, DC 20546–0001

10. SPONSORING/MONITORING AGENCY REPORT NUMBER

NASA TM–107028

11. SUPPLEMENTARY NOTES

Responsible person, Robert G. Deissler, organization code 0130, (216) 433–5823.

12a. DISTRIBUTION/AVAILABILITY STATEMENT

Unclassified - Unlimited
Subject Category 34

This publication is available from the NASA Center for Aerospace Information, (301) 621–0390.

12b. DISTRIBUTION CODE

13. ABSTRACT ***(Maximum 200 words)***

Several turbulent and nonturbulent solutions of the Navier-Stokes equations are obtained. The unaveraged equations are used numerically in conjunction with tools and concepts from nonlinear dynamics, including time series, phase portraits, Poincaré sections, Liapunov exponents, power spectra, and strange attractors. Initially neighboring solutions for a low-Reynolds-number fully developed turbulence are compared. The turbulence is sustained by a nonrandom time-independent external force. The solutions, on the average, separate exponentially with time, having a positive Liapunov exponent. Thus, the turbulence is characterized as chaotic. In a search for solutions which contrast with the turbulent ones, the Reynolds number (or strength of the forcing) is reduced. Several qualitatively different flows are noted. These are, respectively, fully chaotic, complex periodic, weakly chaotic, simple periodic, and fixed-point. Of these, we classify only the fully chaotic flows as turbulent. Those flows have both a positive Liapunov exponent and Poincaré sections without pattern. By contrast, the weakly chaotic flows, although having positive Liapunov exponents, have some pattern in their Poincaré sections. The fixed-point and periodic flows are nonturbulent, since turbulence, as generally understood, is both time-dependent and aperiodic.

14. SUBJECT TERMS

Turbulence; Chaos; Nonlinear; Time series

15. NUMBER OF PAGES

40

16. PRICE CODE

A03

17. SECURITY CLASSIFICATION OF REPORT	18. SECURITY CLASSIFICATION OF THIS PAGE	19. SECURITY CLASSIFICATION OF ABSTRACT	20. LIMITATION OF ABSTRACT
Unclassified	Unclassified	Unclassified	